Investigation into the Use of ELG for Stand Alone Power System Frequency Control

By Feng Chen

Supervised by Dr. Krishnamoorthy Natarajan

December, 2005

A Thesis submitted in partial fulfillment of the requirements of

the Msc. Eng. Degree in

Control Engineering

Faculty of Engineering

Lakehead University

Thunder Bay, Ontario

Your file Votre référence
ISBN: 978-0-494-15611-7
Our file Notre référence
ISBN: 978-0-494-15611-7

Abstract

The use of ELG for stand alone power system frequency control is investigated in this thesis. Characteristics of a stand alone power system with PCR-ELG are presented. Dynamic simulation of the system is developed using Simulink/SimPowerSystems and is verified by comparing the simulation results with experimental results in the literature. The simulation results show that terminal waveforms of the synchronous machine with controller rectifier load are highly distorted. Pulses in phase voltage caused by negative current through thyristors affect rectifier control if appropriate snubber/filter is not imposed. Based on the simulation results, PCR-ELG control with feedback loop is designed. The control results are compared with those of the system having only normal governing and excitation systems. The results show that PCR-ELG can provide much better frequency control for a stand alone power system than normal governing and excitation control.

Acknowledgment

Dr. K. Natarajan's extreme help and guidance made this work possible. I sincerely appreciate his help and support.
I gratefully acknowledge Dr. X. Liu for the advice.

Contents

List of Figures

List of Tables

Chapter 1

Introduction

1.1 Motivation

Mini-hydro turbines (250kW range) with synchronous generators are being paralleled with diesel plants in remote communities in North-Western Ontario to reduce diesel generation, setting up an autonomous stand alone power system as in Fig. 1-1. The battery bank is charged when the generators serve the system normally and is used to supply the load in an emergency when the generators are cut off. The speed response of hydro turbines to load change is slow and hence it is hard to meet tight frequency standards. Due to the slow hydro turbine response, the synchronous generator could be loaded with an electronic load governor (ELG). This ELG is used to absorb fast load variations to maintain the autonomous network frequency within specification while the exciter is used to control voltage as shown in Fig. 1-2. Random changes in load are common in power systems, with subsequent change of frequency. The power absorbed by ELG can be adjusted quickly to load change, maintaining a balance between the total electrical torque and the hydraulic input torque from the turbine and enabling rapid frequency control. Electronic load governors are commercially available in three types: Zero-crossing contactor based banks of resistive loads (ZC-ELG), three phase controlled resistive loads (PC-ELG) and phase controlled rectifier with resistive load (PCR-ELG).

ZC-ELG and PC-ELG introduce no harmonics, but lack fine control. The control of ELGs in autonomous networks with loose voltage and frequency deviation standards (for developing countries) has been studied in [1] using ZC-ELG and the results show poor applicability of this method for networks with tight standards. In [1], a full load rejection test was performed using ZC-ELG, and the frequency rise about 20% at its peak. It was thus considered necessary to improve the response of the ELG.

In this thesis, a phase controlled rectifier with a resistive load (PCR-ELG) is chosen as electronic load governor. The studied system is shown in Fig. 1-2. It is a synchronous generator with PCR-ELG, in which the hydro turbine powers the generator. Field voltage is provided by the exciter while the governor controls water flow to the hydro turbine. Control of PCR-ELG with a feedback loop is necessary to balance power during load change and can lead to better performance of the system upon combining with the governor and exciter. Experimental results in [2], [3], [4] indicate that terminal voltages and currents of a synchronous machine with rectifier-load are highly distorted due to glitches caused by line current commutation. Output of the synchronous generator in this system must therefore be analyzed.

The main objective of this thesis is to design the controller for PCR-ELG. Initially, dynamic simulation of the hydro turbine, synchronous generator and autonomous network load along with a PCR-ELG is developed and verified using experimental results available in the literature. The transient and steady state characteristics of the system are analyzed. Finally, a PCR-ELG controller along with a feedback loop is designed based on the simulation results.

1.2 Background

A peculiarity of the system shown in Fig. 1-2 is the fact that the synchronous generator has controlled rectifier-load: It feeds a reactive DC load through a controlled rectifier. In a large network with many large generators, a synchronous machine can be represented

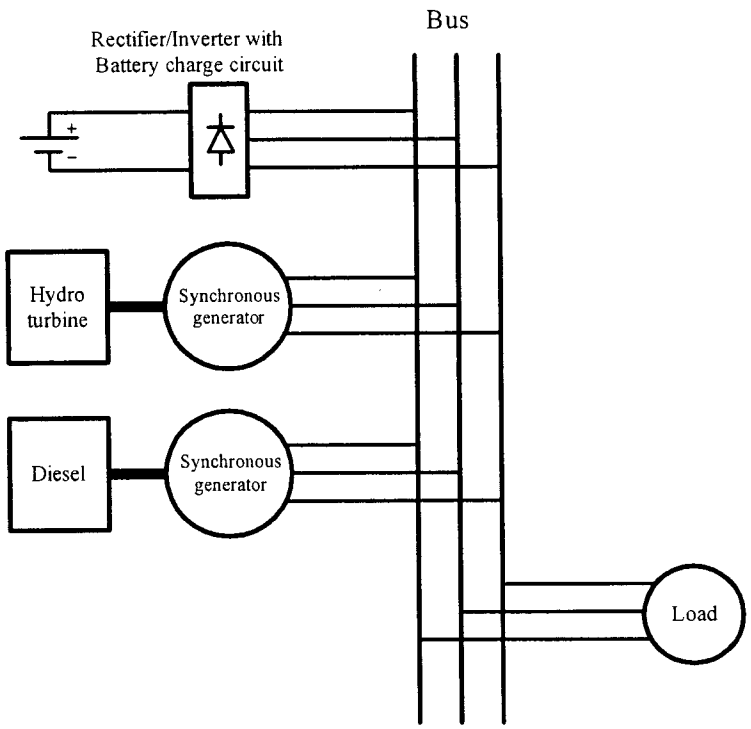

Figure 1-1: A block diagram of autonomous power system

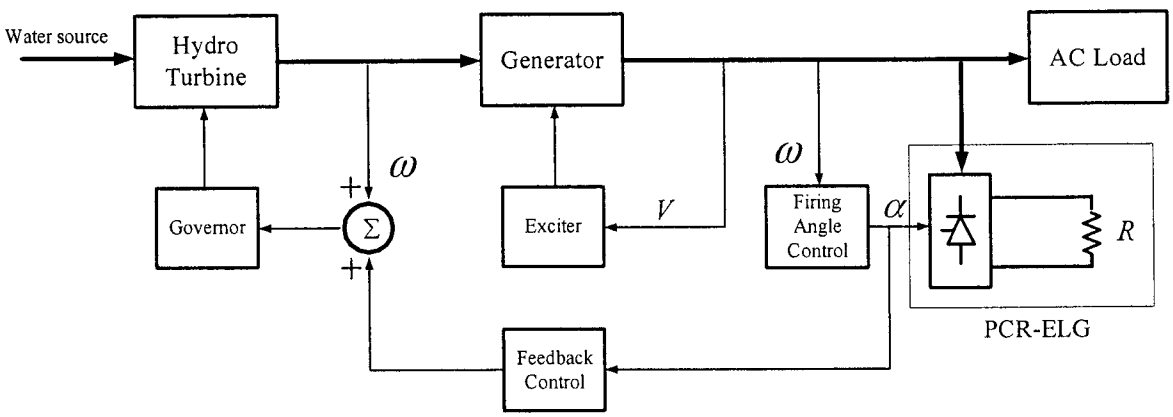

Figure 1-2: Block diagram of the studied system.

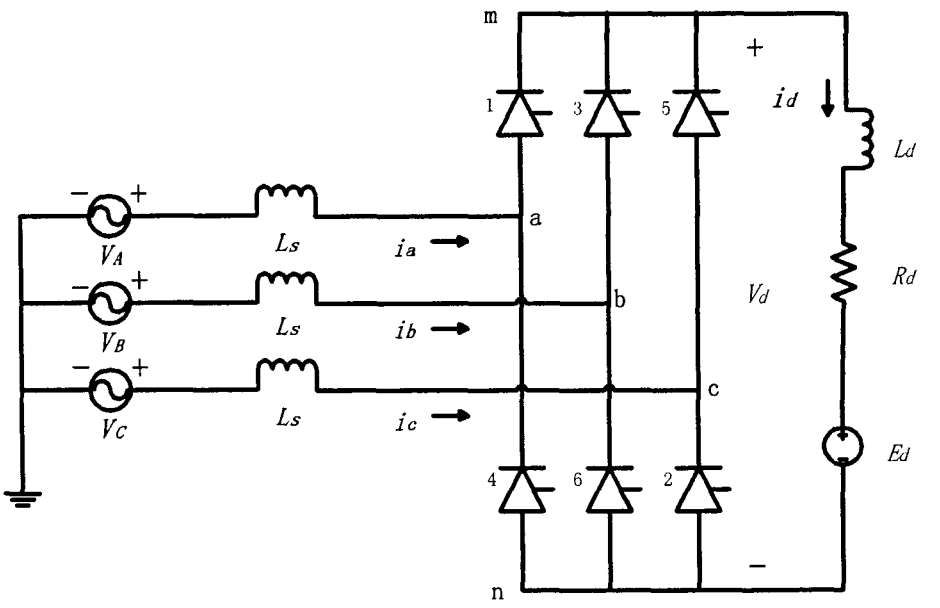

Figure 1-3: Ideal three-phase voltage source feeding DC load with back-EMF through a thyristor converter

by an ideal voltage source and Fig. 1-3 would represent a simplified circuit diagram of a synchronous generator feeding DC load with back-EMF through a thyristor converter. The controlled rectifier consists of six thyristors, numbered 1 through 6 and connected in a full bridge configuration. V_A, V_B and V_C are sinusoidal voltages with amplitude V_p and a phase shift of 120° with respect to one another. The inductances, L_s, normally represent transformer or power line leakage inductance, and need to be placed in series with ideal voltage sources. If the dc current is assumed to be constant value I_{dc}, the average value of the output dc voltage can be expressed as [5]:

$$V_{dc} = \frac{3\sqrt{3}}{\pi} V_p \cos(\alpha) - \frac{3\omega L_s}{\pi} I_{dc} \tag{1.1}$$

where α is the firing angle.

Equation (1.1) does not contain any information about the voltage ripple at the dc

side, but it can be used to calculate the dc side average power.

Fig. 1-4 shows the simulation results for the system in Fig. 1-3. It is a valve by valve detailed simulation. The parameters are provided in Table 1.1. The terminal waveforms of the generator that is loaded with a RL load through a rectifier with a firing angle of 45° are shown in Fig. 1-4. During each commutation, two out of three phase voltages are shorted together by the converter thyristor through the inductor in each phase. For each line voltage, this happens twice per cycle, resulting in deep notches down to zero. For example, V_{ca} goes to zero during the commutation from thyristors 2 to 4 as from points E to F shown in the line voltage waveform in Fig. 1-4. There are four other notches where one of the other two phases is involved in commutation. As a consequence of applied voltages, there are glitches at phase current peak.

Table 1.1 Parameters for C code simulation		
$\alpha = \pi/4$	$L_s = 0.045mH$	$V_{LL} = 208V(rms)$
$R_d = 0.5\Omega$	$L_d = 1.33mH$	$E_d = 0V$

It is to be noticed from Fig. 1-4 that there are pulses in phase voltages. All these pulses happen when the thyristors turn off. Sometimes the pulses are large enough to forward bias the thyristors. Take an example to explain how the pulses happen and how they affect the firing angle control. For thyristor 4 in Fig. 1-3, turn-off commences when thyristor 6 is turned on at, let us say, t=0 shown in Fig.1-4. Points a and b Fig. 1-3 are shorted together by thyristors 4 and 6. The commutation of current from thyristors 4 to 6 will not be instantaneous due to inductance L_s in phase a and phase b, and V_{ab} is zero during the commutation as explained earlier. Thyristor current and voltage waveforms during turn-off are shown in Fig. 1-5 [5] . Turn-off of a thyristor requires that it be reverse biased by external circuit for a minimum time period. As we notice in Fig. 1-5, when a thyristor is turned off, the current through it starts decreasing at a fixed rate di_R/dt, which is governed by the external circuit. It continues to decrease and passes through zero and then grows toward negative value. The voltage across the thyristor

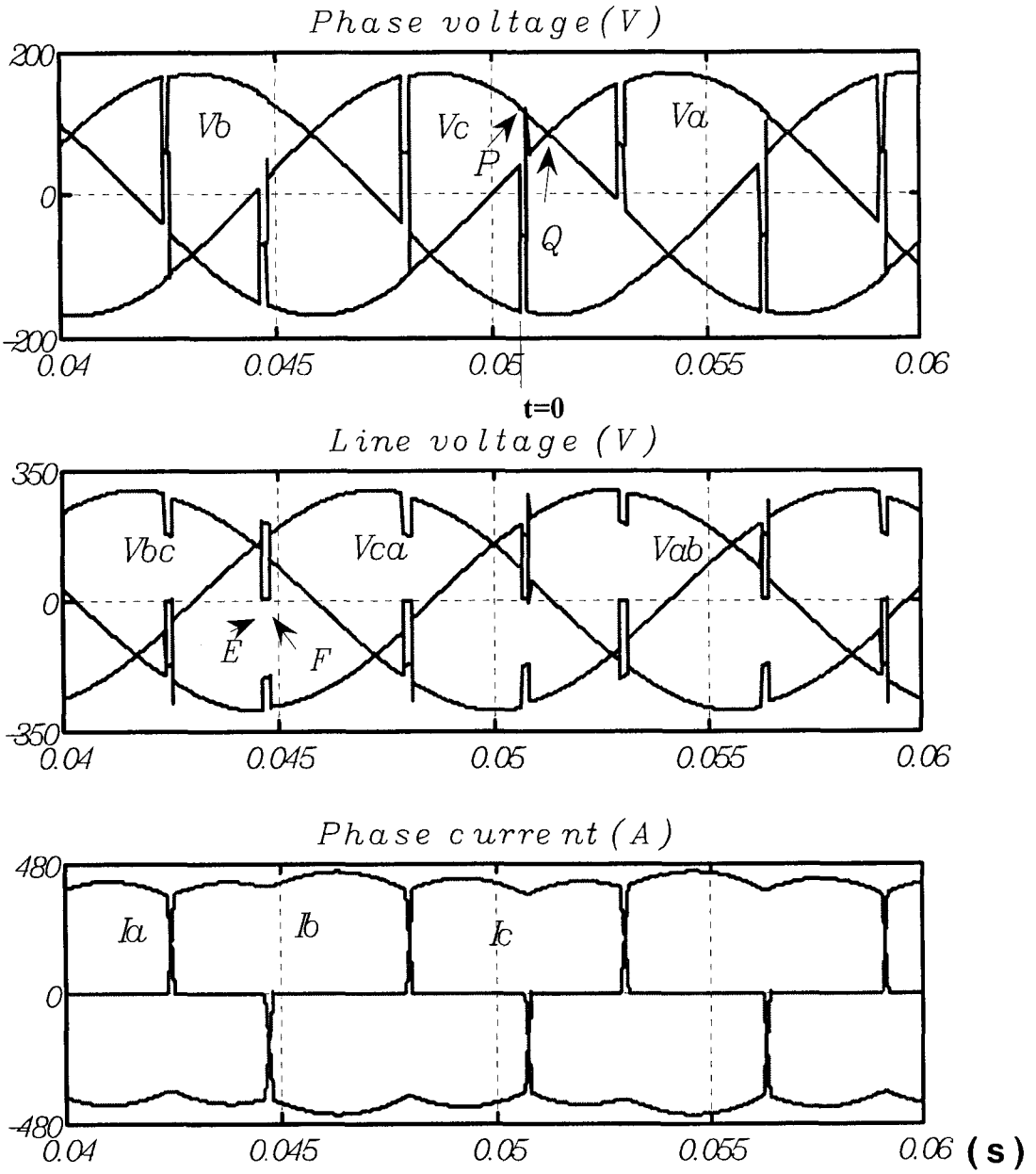

Figure 1-4: Phase voltage, line voltage and phase current of ideal three phase supply fed rectifier operation with RL load at 45 degree & with line inductance.

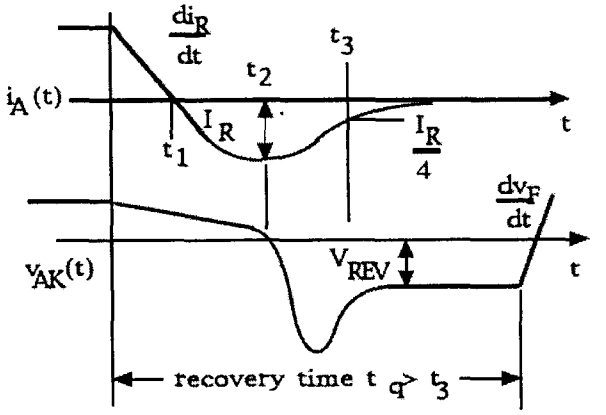

Figure 1-5: Thyristor voltage and current waveforms during turn-off [5]

remains small and positive until t_2. After t_2 the current begins to decay back toward zero. It is this negative current in thyristors that makes pulses in V_a, V_b and V_c. From Fig. 1-3,

$$V_a = V_A - L_s\frac{di_a}{dt} = V_A + L_s\frac{di_R}{dt} \tag{1.2}$$

where i_R is the current of thyristor 4. Before t_2, di_R/dt is negative and therefore V_a is smaller than the sinusoidal V_A. This causes a notch in V_a as shown in Fig. 1-4. At or shortly after time t_2, di_R/dt becomes positive. Hence V_a becomes greater than V_A. This results in a pulse in V_a as shown at point P in Fig. 1-4. How large the pulse is depends on value of L_s and di_R/dt. If higher than V_c, the pulse will forward-bias thyristor 1 earlier which is supposed to be forward-biased at point Q. In practice, the pulses in phase voltages therefore can affect the rectifier control if appropriate snubber/filter are not imposed.

A stand alone synchronous generator however is not an ideal voltage source, and it is even less so if it is characterized by a large value of inductance. Synchronous machine fed load commutated converters are used in a wide variety of applications including shipboard and aircraft dc power distribution systems [6], high power dc supplies [7], and excitation systems of large electric generators [8]. The dynamic modeling of synchronous

machine fed line commutated converters have been studied by researcher. Solutions generally fall into two broad categories: average model and detailed model. Various average models have been derived in [9], [10], [11], [12]. These methods model rectifiers in rotor reference frame exclusively. In such models, without fast electrical transients periodically excited by semiconductor switching, the state variables are constant in the steady state and ac side current glitches caused by line current commutation as well as switching transient at dc side are hidden due to the frame choice. In each of the synchronous machine load commutated converter average models mentioned heretofore the angular velocity of the rotor has been assumed to be constant making Park's equations for the machine linear [9] [10]. However in our stand alone application the angular velocity of the rotor is a controlled variable and it can not be assumed constant. In the second category [13] [14], detailed simulation is available in differential-equation-based languages such as Matlab/Simulink or ACSL. Detailed simulations that include all synchronous machine dynamics, dc link dynamics, and semiconductor switching states yield very accurate results. Because detailed simulations combine presence of fast stator electrical transients and slower mechanical and rotor electrical transients, they are computationally intensive. However, with new generation computers, computation time of detailed models is currently acceptable.

The IEEE Working Group on Prime Mover and Energy Supply Models for System Dynamic Performance Studies provides extensive analysis of hydro turbine modeling and control in [15]. Hydro turbine modeling and governing has also been discussed in [16] [17]. Synchronous generator excitation system has been studied in [18]. The control of ELGs in autonomous networks with loose voltage and frequency deviation standards (for developing countries) has been studied in [1] using ZC-ELG and the results show poor applicability of this method for networks with tight standards.

Krause [19] and Anderson [20] provide details of synchronous machine modeling and control system. Anderson [20] also provides typical system data for use in studies such as those undertaken in this thesis.

1.3 Outline of the Thesis

This thesis consists of five chapters including the Introduction. The chapters are outlined below:

Chapter 2: Modeling of the system

The aim of this chapter is to set up dynamic simulation models of the system studied. The simulation modules include: hydro turbine, synchronous generator, controlled rectifier, and load. The models are interfaced using Matlab/Simulink/SimPowerSystems in a p.u system.

Chapter 3: Verification of model by transient and steady state analysis

Simulation results are compared with the experimental results from the literature to verify the dynamic model developed for control design. This model is then used to analyze transient and steady state behavior of synchronous machine fed load commutated converters and a synchronous generator with simultaneous parallel ac load.

Chapter 4: Control design

This chapter considers the closed-loop control design procedure. Firstly hydro turbine speed governing system and synchronous generator excitation system are reviewed. Since these controllers have been widely used in the power system industry for a long time, only the main conclusions and results are presented. A PI controller for the PCR-ELG is given and a feedback control strategy is evolved to use both PCR-ELG and gate controls on the hydro turbine to regulate the frequency of the system. Transient simulation results are shown and compared with those using only a normal governor and exciter. Validity of these controllers are confirmed through simulation of transient operation in an autonomous power system.

Chapter 5: Conclusions

This chapter includes a summary of the results of this thesis. Concluding remarks give an overview of the thesis. The author's views on future work emanating from the thesis are provided.

Chapter 2

Modeling of the system

A detailed computer simulation is needed to provide insight that allows potential design flaws to be identified before catastrophic failure occurs. The model should include synchronous machine dynamics, dc link dynamics, and semiconductor switching states. The system considered is shown in Fig. 2-1 (no feedback controllers are included). The synchronous machine and hydro turbine are nonlinear and the controlled-rectifier is also a strongly nonlinear switching equipment. So the key problem in modeling is to represent these three components and interface them. The principal subject of this chapter is to describe the models of synchronous machines, hydro turbines and rectifiers available from the literature and develop the interface technique in Matlab/Simulink/SimPowerSystems package.

2.1 Per unit system

The per unit system is widely used in the power system industry to express values of voltages, currents, powers, and impedances of various power equipments. It is mainly used for transformers, ac machines and high voltage transmission lines. The main reasons for using the per unit system are:

1. The values of impedances expressed in p.u. are assumed to stay fairly constant

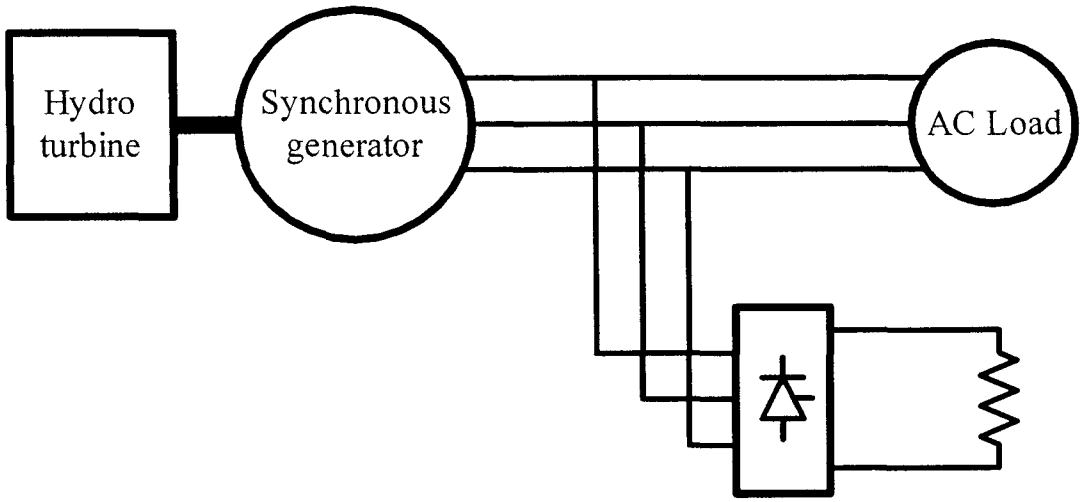

Figure 2-1: Hydro turbine driven synchronous generator with simultaneous ac and rectified dc load

whatever the power and voltage ratings of the generators. For example, for salient pole synchronous machines, the synchronous reactance X_d is generally between 0.60 and 1.50 p.u., whereas the subtransient reactance X_d'' is generally between 0.20 and 0.50 p.u. The per unit system enables choice of parameters for a synchronous machine when explict data is not available.

2. When values are expressed in p.u., the comparison of electrical quantities with their normal values is straightforward. For example, a transient voltage reaching a maximum of 1.42 p.u. indicates immediately that this voltage exceeds the nominal value by 42%.

In a power system, once base Volt.amp and base voltage are selected, all parameters and variables are normalized using these base quantities. Usually, when the machine is being considered separately, the base Volt.amp is selected as the rating of the machine. The rms value of the rated phase voltage is generally selected as base voltage for the abc variables while the peak value is generally selected as base voltage for dq0 variables. All the equations and parameters in this thesis are expressed in the per form unless otherwise notified.

2.2 Synchronous machine model

In this section, the mathematical model for a synchronous machine is developed. The synchronous machine under consideration in this thesis is salient pole and has three stator windings, one field winding, one d-axis damper winding and one q-axis damper winding, as shown in Fig. 2-2. A generator is represented by its torque equations and voltage equations [19].

2.2.1 Voltage equation

In studying power systems, researchers tend to regard the generator as an ideal voltage in series with an RL impedance, which implements the internal impedance of the machine. This model in Fig. 2-3 is called the simplified model and works well only in the case of infinite bus. Since the system we consider is a stand alone power system, the detailed model, which takes into account all relevant dynamic phenomena occurring in the machine, is needed for the purpose of analysis. The synchronous machine under consideration is a salient pole and has three stator windings, one field winding, one d-axis damper winding and one q-axis damper winding. The windings are magnetically coupled. The magnetic coupling between the windings is a function of the rotor position. Thus the flux linking each winding is also a function of the rotor position. The instantaneous terminal voltage of any winding is in the form,

$$v = -ri - \frac{d\lambda}{dt} \tag{2.1}$$

where r is the winding resistance, i is the current and λ is the flux linkage. It is assumed that the direction of positive stator current is out of the terminals since the synchronous machine under consideration is a generator. The expressions of the winding voltages are complicated because of the variation of λ with the rotor position.

In the late 1920s, Park [21] [22] formulated change of variables which replaced the variables associated with the stator windings of a synchronous machine with fictitious

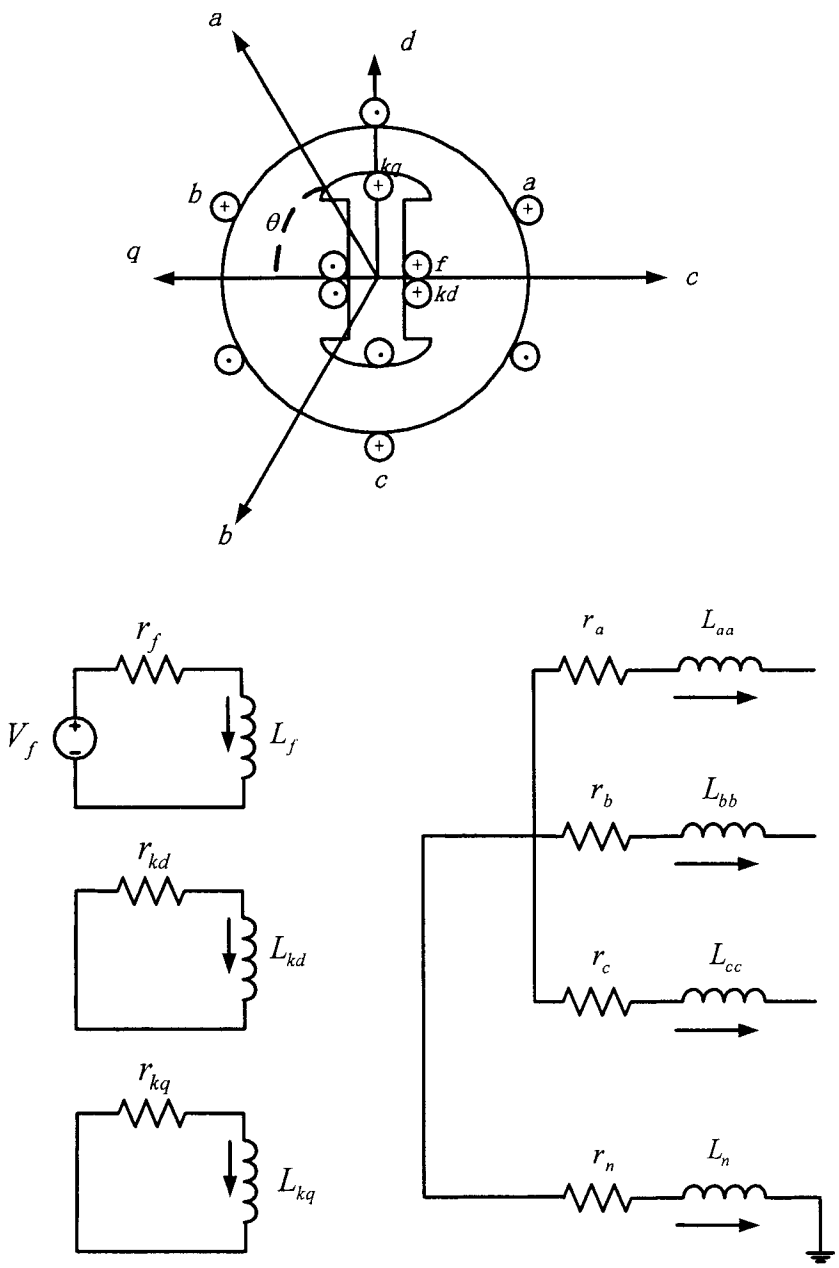

Figure 2-2: Schematic diagram of a synchronous machine

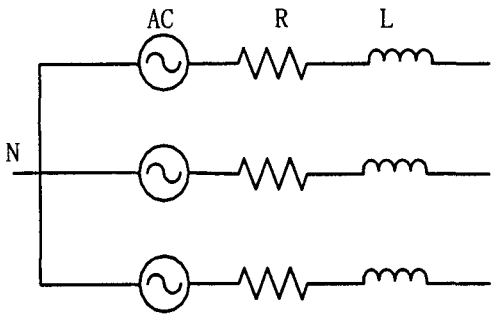

Figure 2-3: Simplified synchronous machine model

windings rotating with the rotor. In other words, the stator variables are referred to the frame of reference fixed in the rotor. The new quantities are obtained from the projection of the actual variables on three axes: One along the direct axis of the rotor field winding, called the direct axis; a second along the neutral axis of the field winding, called the quadrature axis; and the third on a stationary axis. Park's transformation eliminates the time varying inductions from the voltage equations and simplifies the mathematical description of a synchronous machine. There exist a couple of forms of Park's transformation in the literature. In this work, the Park's transformation used is defined as [19]

$$K = \frac{2}{3}\begin{bmatrix} \cos\theta & \cos\left(\theta - \frac{2}{3}\pi\right) & \cos\left(\theta + \frac{2}{3}\pi\right) \\ \sin\theta & \sin\left(\theta - \frac{2}{3}\pi\right) & \sin\left(\theta + \frac{2}{3}\pi\right) \\ \frac{1}{2} & \frac{1}{2} & \frac{1}{2} \end{bmatrix} \tag{2.2}$$

where θ is the displacement between the q-axis and a-axis shown in Fig. 2-2 and

$$v_{qd0} = K v_{abc} \tag{2.3}$$

where

$$v_{qd0} = \begin{bmatrix} v_q \\ v_d \\ v_0 \end{bmatrix} \text{ and } v_{abc} = \begin{bmatrix} v_a \\ v_b \\ v_c \end{bmatrix} \tag{2.4}$$

The inverse park's transformation is

$$K^{-1} = \begin{bmatrix} \cos\theta & \sin\theta & 1 \\ \cos\left(\theta - \frac{2}{3}\pi\right) & \sin\left(\theta - \frac{2}{3}\pi\right) & 1 \\ \cos\left(\theta + \frac{2}{3}\pi\right) & \sin\left(\theta + \frac{2}{3}\pi\right) & 1 \end{bmatrix} \tag{2.5}$$

and

$$v_{abc} = K^{-1} v_{qd0} \tag{2.6}$$

The angle θ is given by

$$\theta = \int_0^t \omega_r(\xi)\, d\xi + \theta(0) \tag{2.7}$$

where ω_r is the electrical angular velocity of the rotor and ξ is a variable of integration. It should be noted that ω_r is equal to the electrical angular velocity of the terminal voltage in isolated operation.

Park's voltage equations are often written in following form [19].

$$v_q = -r_s i_q + \frac{\omega_r}{\omega_b}\psi_d + \frac{\rho\psi_q}{\omega_b} \tag{2.8}$$

$$v_d = -r_s i_d - \frac{\omega_r}{\omega_b}\psi_q + \frac{\rho\psi_d}{\omega_b} \tag{2.9}$$

$$v_0 = -r_s i_0 + \frac{\rho\psi_0}{\omega_b} \tag{2.10}$$

$$v_{fd} = r_{fd} i_{fd} + \frac{\rho\psi_{fd}}{\omega_b} \tag{2.11}$$

$$v_{kd} = r_{kd} i_{kd} + \frac{\rho\psi_{kd}}{\omega_b} \tag{2.12}$$

$$v_{kq} = r_{kq} i_{kq} + \frac{\rho\psi_{kq}}{\omega_b} \tag{2.13}$$

where ρ is the operator d/dt. The flux linkages per second are expressed as:

$$\begin{aligned}
\psi_q &= -X_l i_q + X_{mq}(-i_q + i_{kq}) \\
\psi_d &= -X_l i_d + X_{mq}(-i_d + i_{fd} + i_{kd}) \\
\psi_0 &= -X_0 i_0 \\
\psi_{fd} &= X_{lfd} i_{fd} + X_{md}(-i_d + i_{fd} + i_{kd}) \\
\psi_{kd} &= X_{lkd} i_{kd} + X_{md}(-i_d + i_{fd} + i_{kd}) \\
\psi_{kq} &= X_{lkq} i_{kq} + X_{mq}(-i_q + i_{kq})
\end{aligned} \tag{2.14}$$

Park's equations can be expressed in following matrix form.

$$\begin{aligned}
\begin{bmatrix} v_q \\ v_d \\ v_0 \\ v_{fd} \\ v_{kd} \\ v_{kq} \end{bmatrix} = &\begin{bmatrix} -r_s & -\omega_r X_d & 0 & \omega_r X_{md} & \omega_r X_{md} & 0 \\ \omega_r X_q & -r_s & 0 & 0 & 0 & -\omega_r X_{mq} \\ 0 & 0 & -r_s & 0 & 0 & 0 \\ 0 & 0 & 0 & r_{fd} & 0 & 0 \\ 0 & 0 & 0 & 0 & r_{kd} & 0 \\ 0 & 0 & 0 & 0 & 0 & r_{kq} \end{bmatrix} \begin{bmatrix} i_q \\ i_d \\ i_0 \\ i_{fd} \\ i_{kd} \\ i_{kq} \end{bmatrix} \\
&+ \frac{1}{\omega_b} \begin{bmatrix} -X_q & 0 & 0 & 0 & 0 & X_{mq} \\ 0 & -X_d & 0 & X_{md} & X_{md} & 0 \\ 0 & 0 & X_l & 0 & 0 & 0 \\ 0 & -X_{md} & 0 & X_{fd} & X_{md} & 0 \\ 0 & -X_{md} & 0 & X_{md} & X_{kd} & 0 \\ -X_{mq} & 0 & 0 & 0 & 0 & X_{kq} \end{bmatrix} \begin{bmatrix} i'_q \\ i'_d \\ i'_0 \\ i'_{fd} \\ i'_{kd} \\ i'_{kq} \end{bmatrix} \text{ pu}
\end{aligned} \tag{2.15}$$

where

ω_r: rotor angular velocity;

v_d: stator d-axis terminal voltage;

v_q: stator q-axis terminal voltage;

v_0: stator zero axis terminal voltage;

i_d: stator d-axis terminal current;

i_q: stator q-axis terminal current;

i_0: stator zero axis terminal current;

v_{fd}: field winding terminal voltage (reflected to the stator);

i_{fd}: field winding terminal current (reflected to the stator);

i_{kd}: d-axis damper winding current (reflected to the stator);

i_{kq}: q-axis damper winding current (reflected to the stator);

r_s: stator phase resistance;

r_{fd}: field winding resistance (reflected to the stator);

r_{kd}: d-axis damper resistance (reflected to the stator);

R_{kq}: q-axis damper resistance (reflected to the stator);

X_d: d-axis reactance;

X_q: q-axis reactance;

X_0: zero axis reactance;

X_{md}: d-axis coupling reactance;

X_{mq}: q-axis coupling reactance;

X_{fd}: field winding reactance;

X_{kd}: d-axis damper winding reactance (reflected to the stator);

X_{kq}: q-axis damper winding reactance (reflected to the stator);

The synchronous machine's equivalent circuit in rotor reference frame is shown in Fig. 2-4 [19].

Several comments can be made regarding (2.15).

1. In the case of a Y-connected generator without neutral connection, zero variables are equal to zero and therefore excluded from the equations.

2. v_{kd} and v_{kq} are equal to zero.

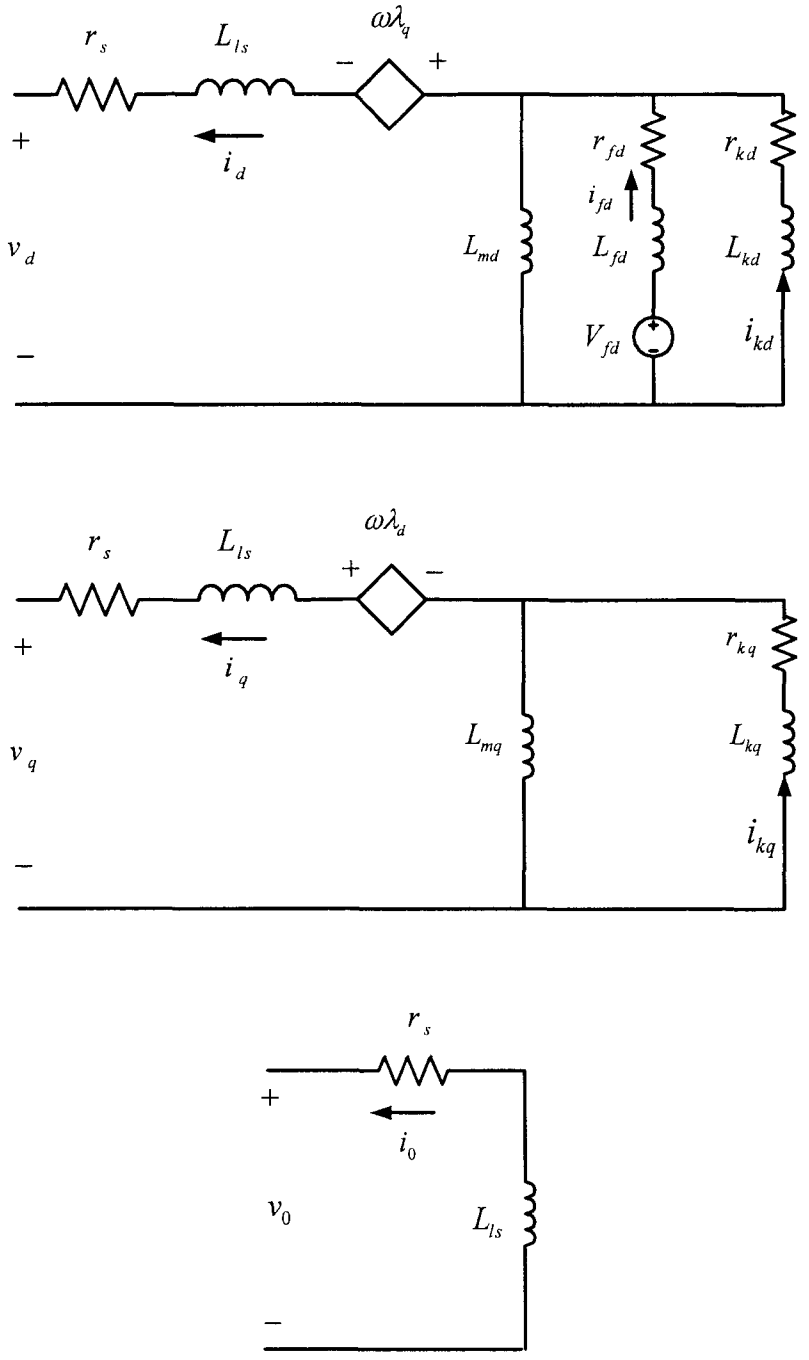

Figure 2-4: Synchronous machine's equivalent circuit in rotor reference frame [19]

3. Because of the effect of Park's transformation, when the generator is operating in sinusoidal steady state, all voltage, current and flux linkages in (2.15) are dc in steady state.

4. The non-linearity in the above equations derives from the presence of the rotor angular velocity ω_r. If ω_r is assumed to be a constant, (2.15) is linear and can be easily rearranged in the standard state-space linear time invariant system form $\dot{x} = Ax + Bu$.

5. All rotor parameters are already reflected to stator. Therefore, if actual values of rotor variables are of interest, the turns ratio between the rotor and stator needs to be taken into account.

6. Usually in simulation, $E_{fd} = v_{fd}\frac{X_{md}}{r_{fd}}$ is used to define the field voltage rather than the actual voltage applied to the field winding because, with stator open-circuited and in steady-state rated speed operation, one per unit E_{fd} then produces one per unit open-circuit terminal voltage.

2.2.2 Torque equation

Equation (2.15) describes a synchronous generator electrically, however, the mechanical equation of the system is needed in order to complete the mathematical representation of synchronous machines. As shown in Fig. 2-5, T_m, the mechanical torque, acts to increase rotational speed whereas T_e, the electrical torque and T_{loss}, the loss torque, acts to slow it down. If T_{loss} is neglected, when T_m and T_e are equal in magnitude, the rotational speed will be constant. Torque equation governs the motion of the machine rotor relating the accelerating inertia torque to the resultant of the mechanical and electrical torques on the rotor. This equations of the synchronous machine are described by [19]:

$$2H\dot{\omega}_r = T_m - T_e - B\omega_r \tag{2.16}$$

$$T_e = \left(\psi_d i_q - \psi_q i_d\right) \tag{2.17}$$

$$\psi_d = -X_d i_d + X_{md} i_{fd} + X_{md} i_{kd} \tag{2.18}$$

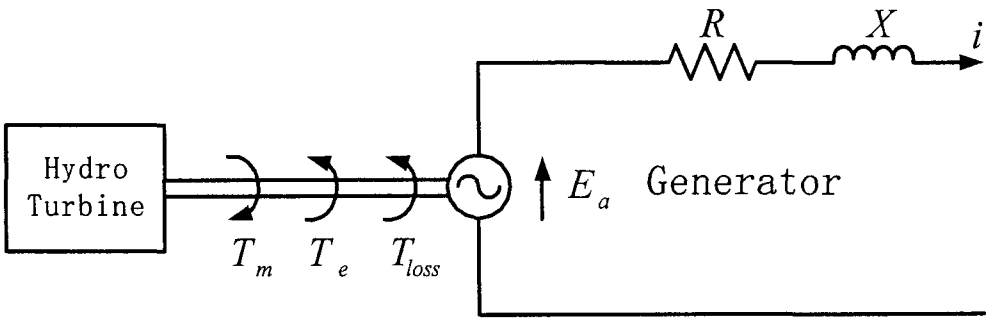

Figure 2-5: Mechanical and electrical torques in a generator

$$\psi_q = -X_q i_q + X_{mq} i_{kd} \tag{2.19}$$

where T_m : mechanical torque

T_e : electrical torque

B : damping factor

ψ_d, ψ_q : d-axis and q-axis flux linkage per second respectively.

H : inertia constant. The inertia constant is expressed in second. For large machines, this constant is around 3 to 5 s. An inertia constant of 3 s means that the energy stored in the rotating part could supply the nominal load for 3 s. For small machines, H is lower. For example, for a 3 HP generator, it can be between 0.5 and 0.7 s.

Note that all the variables in above equations are in per unit except t, which is in seconds.

2.3 Hydro turbine (prime mover) model

Models of hydro turbines were analyzed in [15] by the IEEE Working Group on Prime Mover and Energy Supply Models for System Dynamic Performance Studies. Here, the main assumptions and relevant results to this thesis are summarized.

The block diagram in Fig. 2-6 represents the dynamic characteristics of a hydraulic turbine, with a penstock, unrestricted head and tail race, and with either a very large

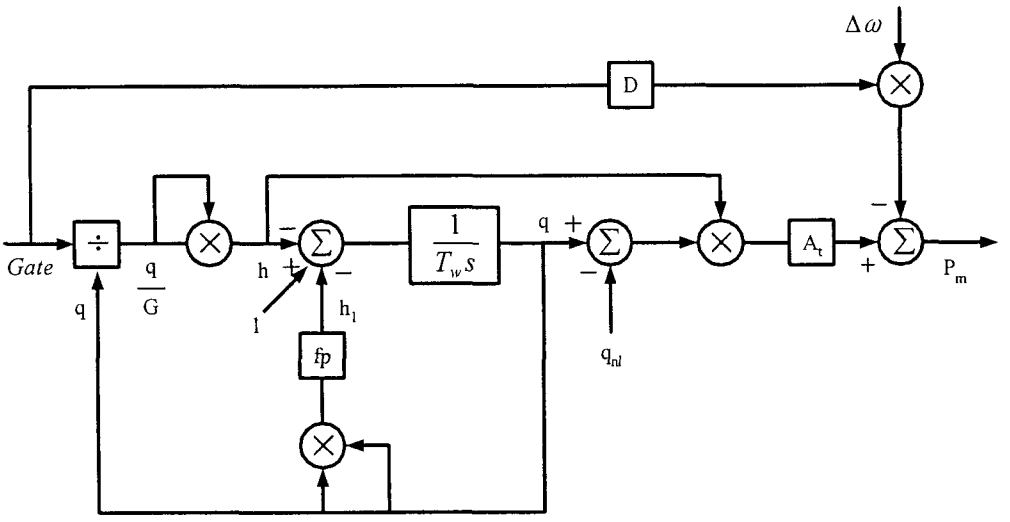

Figure 2-6: Block diagram of non-linear model of hydro turbine [15]

or no surge tank. The penstock is modeled assuming an incompressible fluid and a rigid conduit of length L and cross-section A. Penstock head losses are proportional to flow squared and f_P the head loss coefficient is usually ignored [15].

The rate of change of flow in the conduit is

$$\frac{dq}{dt} = (h_0 - h - h_1)gA/L \tag{2.20}$$

where:

q : turbine flow rate. m^3/s

A : penstock area. m^2

L : penstock length. m

g : the acceleration due to gravity. m/s

h_0 : the static head of water column. m

h : the head of the turbine admission. m

h_1 : the head loss due to friction in the conduit. m

Expressed in per unit with h_{base} as the static head of the water column and q_{base} as

the turbine flow rate with gates fully open and base head, this relation becomes

$$\frac{dq}{dt} = (1 - h - h_1)/T_w \tag{2.21}$$

where T_w is called water time constant or water starting time and is defined as:

$$T_w = \frac{L}{A}\frac{q_{base}}{h_{base}g} \text{ s} \tag{2.22}$$

The per unit flow rate through the turbine is given by:

$$q = G\sqrt{h} \tag{2.23}$$

Per unit turbine power, p_m, on generator MVA base is expressed as

$$P_m = A_t h(q - q_{nl}) - DG\triangle\omega \tag{2.24}$$

where

D : the speed deviation damping coefficient

q_{nl} : the per unit no-load flow, accounting for turbine fixed power losses.

G : the gate opening ($G_{\max} > G > G_{\min}$)

A_t: $1/(G_{\max} - G_{\min})$

2.4 Controlled rectifier model

The controlled rectifier used in this work consists of six thyristors, numbered 1 through 6 and connected in a full bridge configuration shown in Fig. 2-7. Each valve is gated on when a positive voltage is applied to the gate-cathode junction (regardless of whether or not it conducts) and is fired when it is forward biased after being gated on. Many average models can be found in the literature [9], [11], [23] for the study and control of dc side output. However, average models often hide glitches and pulses on the ac side of

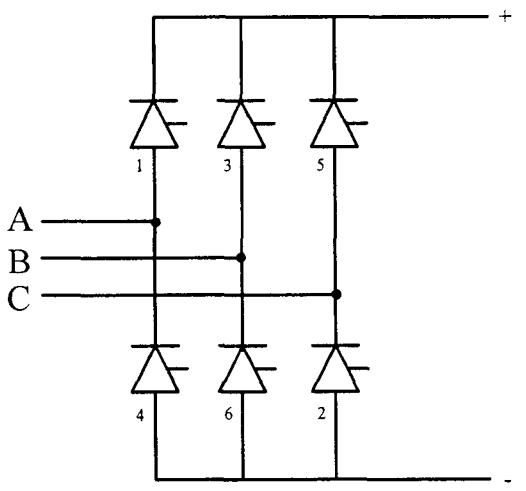

Figure 2-7: Three phase thyristor bridge

rectifiers. Therefore, a detailed valve by valve model is needed when the ac side voltages and currents are to be studied. In this thesis, the controlled rectifier shown in Fig. 2-7 is modeled using Matlab/Simulink/SimPowerSystems in such way that each thyristor is simulated as a resistor Ron, an inductor Lon, and a dc voltage source representing the forward voltage Vf, connected in series with a switch. The switch is controlled by a logical signal depending on the voltage Vak, the current Iak, and the gate signal g, as shown in Fig. 2-8. When a thyristor is forward biased (Vak>0) and a positive gate pulse is applied, it starts to conduct with a small forward voltage Vf across it. It turns off when the current flow into the device becomes 0. When the thyristor is reverse biased (Vak<0), it stays in the off state.

2.5 Load

To make the presentation of the system complete, models of ac and dc loads are given below. In power systems, because loads are mainly inductive, capacitor banks are usually installed at the terminal of networks to improve the power factor. Therefore, to make

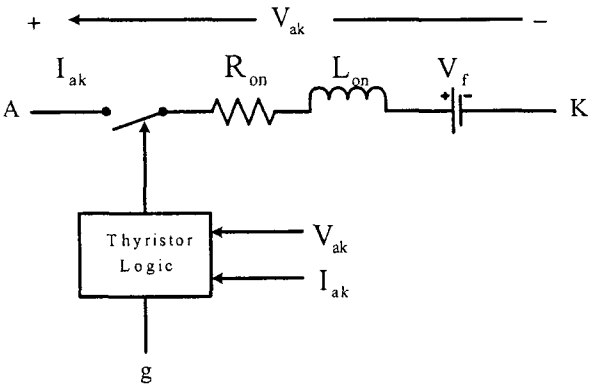

Figure 2-8: A thyristor model

the model development less tedious the ac load in Fig. 2-1 is modeled as resistive. A dc side inductor is often used to filter the harmonics of dc output current or can arise from stray inductance with the dc resistor. The dc load on the controlled rectifier is therefore modeled as

$$v_{dc} = r_{dc} i_{dc} + L_{dc} \frac{di_{dc}}{dt} \tag{2.25}$$

where r_{dc}, L_{dc} are dc side resistor and inductor respectively.

2.6 Interface of the system

In the system shown in Fig. 2-1, interconnection of the hydro turbine and the synchronous generator is straightforward. Hydro turbine's output, mechanical power, is the input of the synchronous generator. The critical problem is how to interface the synchronous generator model in rotor reference frame and the controlled rectifier model in the abc-frame. Equations (2.15) describing a synchronous machine can be written in the standard form

$$\dot{x} = f(x, u, t) \tag{2.26}$$

where $x = [i_q \; i_d \; i_{fd} \; i_{kd} \; i_{kq} \; \omega_r]'$, a vector of the state variables

$u = [v_q \ v_d \ v_{fd} \ v_{kd} \ v_{kq} \ T_m]'$, a vector of the inputs

f = a set of nonlinear functions.

If a synchronous generator is connected to an infinite bus, the system voltages are fixed and can be assumed sinusoidal. Therefore v_q and v_d are constant, and all the inputs in (2.26) are known. (2.26) can be readily solved numerically in rotor reference frame using for example Runge Kutta method [24].

If a controlled rectifier is supplied by an infinite bus power system, its voltage input is fixed and ideal sinusoidal. A full bridge controlled rectifier has twelve different conducting states. For each conducting state, the rectifier with RL load can be modeled in the linear form as

$$\dot{x} = Ax + Bu \tag{2.27}$$

where x : a vector of the state variables

u : a vector of the inputs

Each conducting state results in corresponding different differential equation sets. When the input voltages, v_a, v_b and v_c, are known, a controlled rectifier can be simulated by solving the differential equation which changes every time the rectifier's conducting state changes [25].

The problem here is to interface the two sets of equations both with synchronous machine terminal voltages as inputs and terminal currents as state variables. Besides, they are in different reference frame. Solutions generally fall into two categories. In the first category, these two sets of equations are combined by eliminating synchronous machine terminal voltages. Derivation is difficult and tedious because of the existence of two reference frame. Combined equations are in either the dq-frame or abc-frame. In early literature [2], [3], [4], rectifier loaded synchronous machines are simulated in the abc-frame with assumption of a constant dc side current and electrical angular velocity. However these assumptions hide dc side current ripple. Moreover, because of time-varying machine coefficients these simulations are inefficient. In [9] [11], average models in rotor reference frame are derived, but as mentioned in the last section transient behavior of

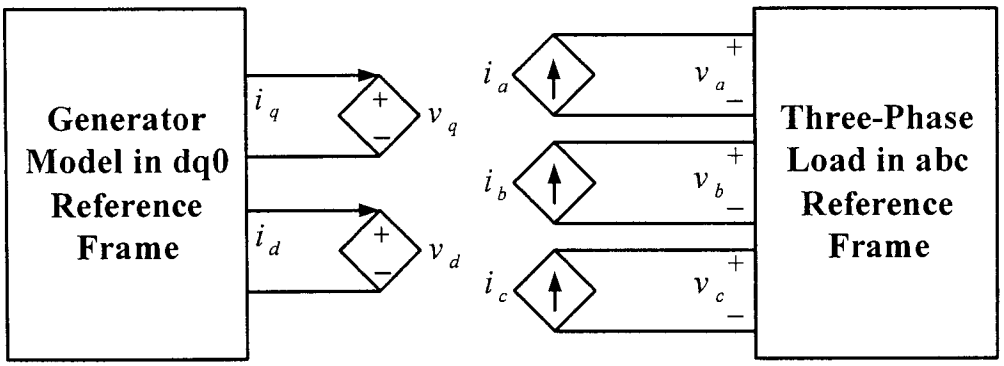

Figure 2-9: Implementation of generator's three-phase output

rectifiers can not be seen using average models.

In the second category, the synchronous machine fed rectifier is simulated by implementing the generator's output with three phase current-dependent current sources shown in Fig. 2-9, which generate currents in the abc-reference frame by calculating them from armature currents in the dq reference frame as

$$\begin{bmatrix} i_a \\ i_b \\ i_c \end{bmatrix} = K^{-1} \begin{bmatrix} i_q \\ i_d \end{bmatrix} \tag{2.28}$$

From the principle of duality, the generator model in the rotor reference frame is loaded with two voltage-dependent voltage sources, representing the generator's armature voltages in dq-reference frame shown in Fig. 2-9, and calculated from the rectifier's input voltages in the abc-reference frame as

$$\begin{bmatrix} v_q \\ v_d \end{bmatrix} = K \begin{bmatrix} v_a \\ v_b \\ v_c \end{bmatrix} \tag{2.29}$$

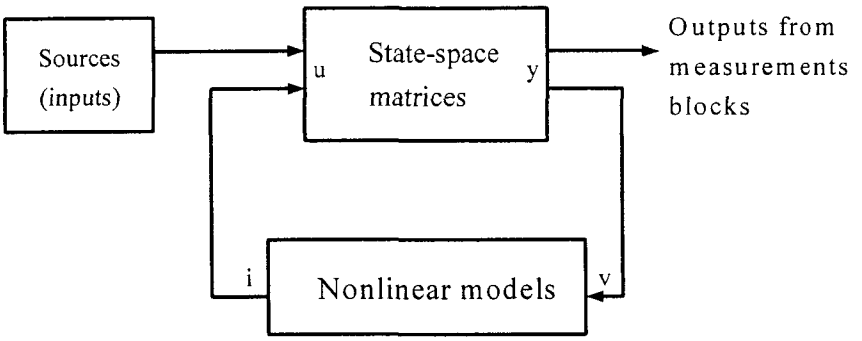

Figure 2-10: Interconnection of Linear Circuit and Nonlinear Models

Simulink/SimPowerSystems by Hydro-Quebec use above idea to interconnect individual modules[13]. In Simulink/SimPowerSystems, each component model is separated into linear or nonlinear models. The state-space representation of all linear parts of the system are obtained using nodal and mesh analysis methods while the nonlinear models are connected in feedback between voltage outputs and current inputs of the linear model. Fig. 2-10 represents the interconnections between linear and nonlinear models.

In this thesis, Simulink/SimPowerSystems is used to interface each component and set up a dynamic model for the system. For the system considered shown in Fig. 2-1, Simulink/SimPowerSystems recomputes the state-space model of the linear circuit, including the main load and the rectifier load, each time the rectifier status changes. Nonlinear synchronous machine model is solved using Runge Kutta method with dq voltage inputs transferred from the abc-reference frame. The dq-current outputs alone with their derivative are transferred into the abc-frame and fed to state-space matrices of the linear circuit.

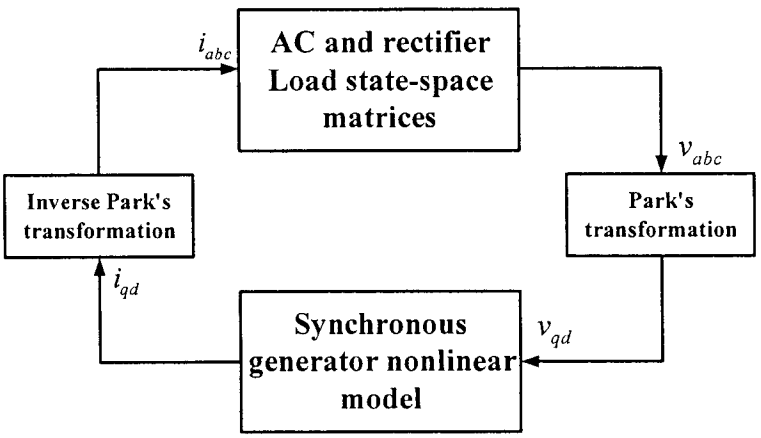

Figure 2-11: Interface of synchronous machine and rectifier load alone with ac load in Matlab/Simulink

Chapter 3

Simulation verification

In order to verify the model described in Chapter 2, the simulation results obtained with it are compared to experimental results in the literature. As this chapter will show, the predictions of the simulations are quite consistent with those of the measurements in [11], [26]. Two types of transients were simulated by the model established in Chapter 2 and compared to the experimental results in [11] and [26]:

1. Transients caused by connection of rectifier load to a synchronous machine which is initially unloaded

2. Transients caused by step change in dc load.

Steady state characteristics are also analyzed. Compared variables included the field current, ac voltage and current, and dc voltage and current. Two different synchronous machines are considered for generality.

The first system used to verify the accuracy of the detailed simulations is depicted in Fig. 3-1. The synchronous machine is initially unloaded and is connected to an RL converter load at t=0.02s. Information regarding the synchronous machine is given in Table 3.1 [10]. In this case, only one damper winding in the q-axis is taken into account. Fig. 3-2 illustrates the simulated dynamic behavior of rectifier loaded synchronous machine following the connection of a dc load to the rectifier (firing angle is zero), while Fig. 3-3 shows the corresponding experimental results from [26]. In Figs. 3-2 and 3-3 the

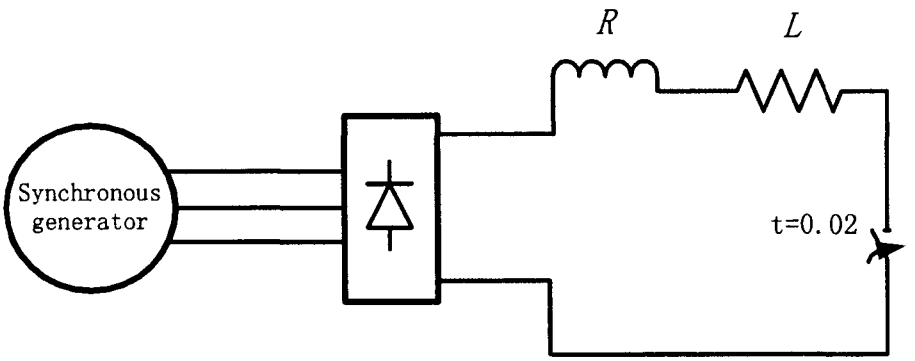

Figure 3-1: System configuration for test I

following variables are plotted: ac voltage v_a, ac current i_a, dc voltage v_{dc} and current i_{dc}. In all figures, the scales of the voltages and currents are in per unit. In this study, it is assumed that the frequency of the synchronous machine remains constant at the rated value.

Table 3.1 Synchronous Machine 1 Parameters				
$r_s = 0.00515$pu	$X_{mq} = 1.00$pu	$r_{kd} = 0.0240$pu	$r_{fd} = 0.0011$pu	$r_{kq} = 0.0613$pu
$X_{ls} = 0.08$pu	$X_{md} = 1.77$pu	$X_{lkd} = 0.334$pu	$X_{lfd} = 0.137$pu	$X_{lkq} = 0.330$pu
$w = 1$pu	$V_{fd} = 1.515$pu	$R = 2$pu	$L = 2$pu	

Initially the synchronous machine fed rectifier system is operating with dc link open with the excitation held fixed at the value that gives 1.52 times rated open-circuit terminal voltage at synchronous speed. It is instructive to observe v_a, i_a, v_{dc} and i_{dc} following dc link load connection. Before the rectifier is loaded, terminal voltage of the synchronous machine is sinusoid and the output voltage of the rectifier is dc with a ripple. The ac and dc current begin to increase immediately after dc load is connected. The dc and phase voltage drop due to non–regulation of excitation and then return to their previous values. Transient die out within 0.02s because slow mechanical system variation is not taken into

account in the assumption of constant ω. In the steady state, there are four large glitches in phase voltage per cycle and larger triangular ripple in dc voltage. It is interesting to observe that after the synchronous machine is loaded with an RL load through the rectifier, phase voltages are highly distorted, the ripple in dc voltage becomes triangular and there is a glitch at the peak of the phase current. All these are due to six current commutations per line frequency cycle in the converter. During each commutation, two of the three phase voltages are shorted together by the converter diodes/thyristors through the inductance in each phase. The line-to-line voltage is short-circuited twice per cycle, resulting in a deep notch.

As we can see from Figs. 3-2 and 3-3, the two sets of waveforms from the simulation and experimental results are virtually identical in both transient and steady state.

Another system depicted in Fig. 3-4 was used to verify the accuracy of the detailed simulation. The parameters of the synchronous machine used therein are given in Table 3.2 [11], where all rotor quantities have been referred to the stator by the appropriate turns ratio. The dc-link capacitor has capacitance of 450μF, and r_1 and r_2 are 32.8Ω and 13.6Ω respectively. In the test of reference [11], the machine was running at an electrical rotor speed of 377rad/s. A 29.9V was applied to the field winding by a constant voltage, essentially zero impedance source. The transient behavior of the system when the switch is closed are predicted by the simulation and experimental results as shown in Figs. 3-5 and 3-6 respectively. Variables depicted are the dc link voltage, the phase current, the dc link current and the field current.

Table 3.2 Synchronous Machine 2 Parameters			
$r_s = 0.382\Omega$	$L_{ls} = 0.8304$mH	$L_{mq} = 13.5$mH	$L_{md} = 39.65$mH
$r_{kd1} = 40.47\Omega$	$L_{lkd1} = 4.732$mH	$r_{kq1} = 31.8\Omega$	$L_{lkq1} = 6.13$mH
$r_{kd2} = 1.308\Omega$	$L_{lkd2} = 3.675$mH	$r_{kq2} = 0.923\Omega$	$L_{lkq2} = 3.4$mH
$r_{kd} = 0.122\Omega$	$L_{lfd} = 2.54$mH	$N_s/N_{fd} = 0.02711$	$P = 4$

As shown in Figs. 3-5 and 3-6, immediately after the switch is closed the dc and

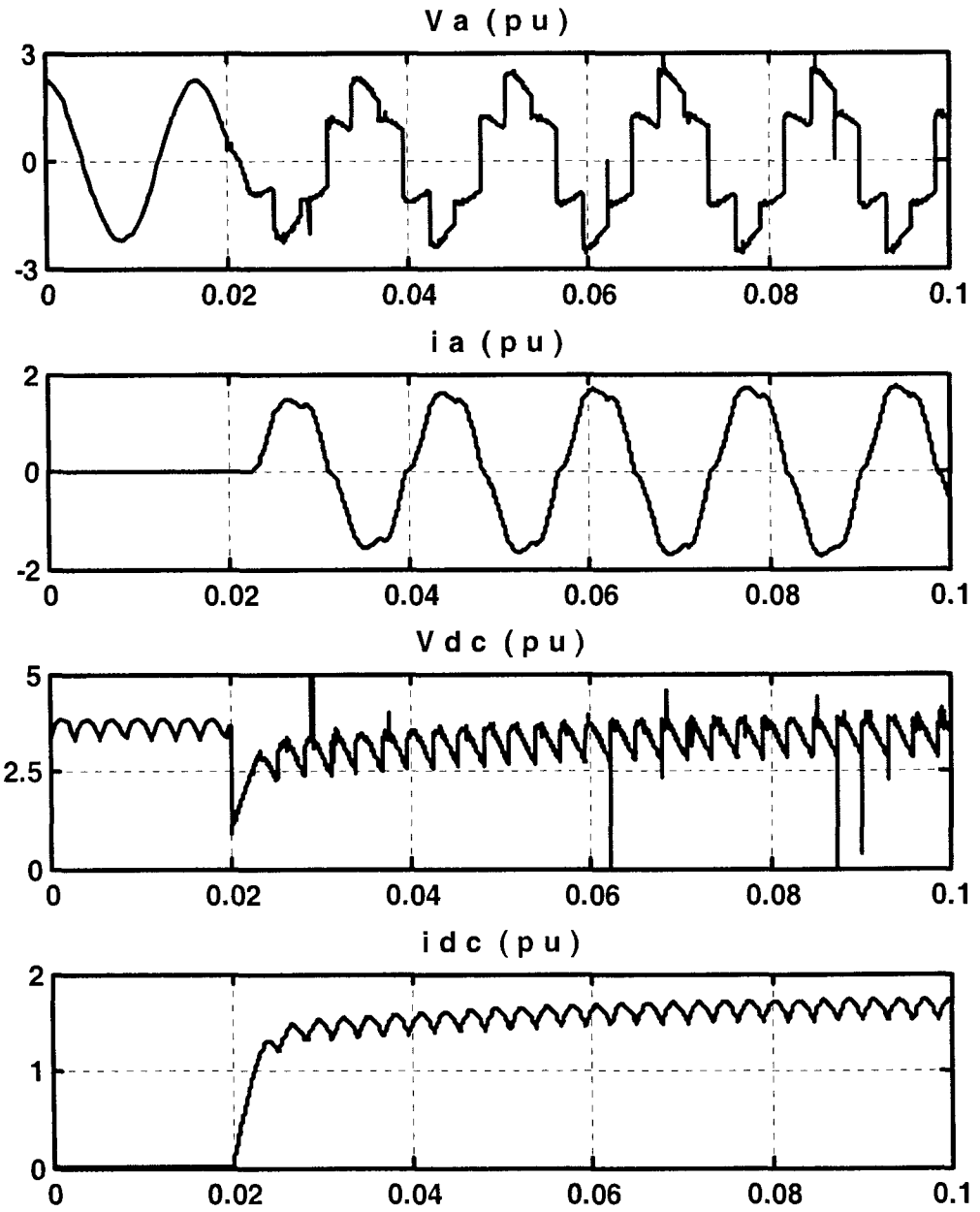

Figure 3-2: Detailed simulation results of a phase voltage, a phase current, dc-link voltage and current.

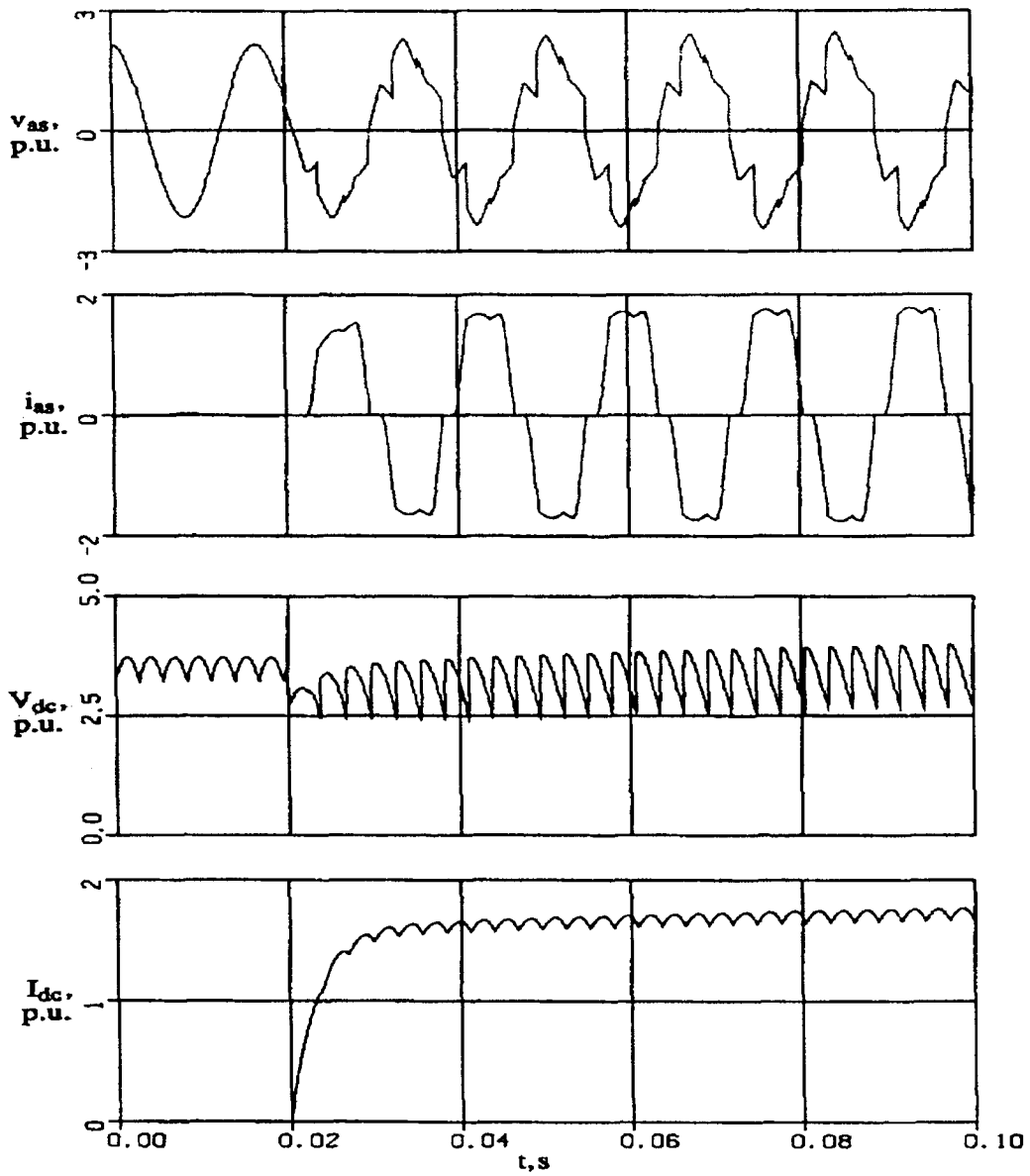

Figure 3-3: Measured results of a phase voltage, a phase current, dc-link voltage and current [26].

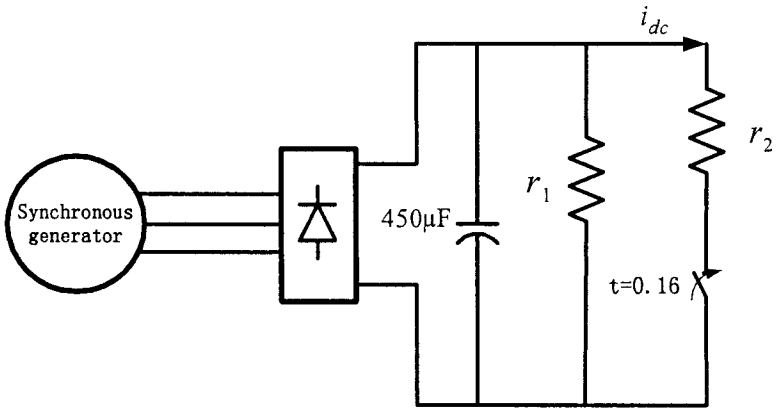

Figure 3-4: System configuration for test II

phase currents increase rapidly. The field current of the generator also increases in order to maintain constant field flux in response to the increased stator current. As the phase, field and damper winding currents decay, the machine flux linkages decrease which causes the synchronous machine back emf and hence the dc-link current to decrease. The dc-link voltage initially decreases sharply then continues to decrease more gradually as the currents decay until a new steady state operating point is reached.

The simulation results closely agree with experimental results throughout the transient and steady state. The differences can be explained by either the generator model's inherent drawbacks (absence of modeling of magnetic saturation and remnant magnetism), or by errors in the main generator's parameters.

The results of the simulation presented in above two examples lead to the following conclusions: Transient and steady state waveforms obtained with the detailed model developed in Chapter 2 are quite consistent with those obtained from experiments. All synchronous machine dynamics, dc link dynamics, and semiconductor switching states can be predicted by the developed dynamic simulation. Based on the above conclusions, the detailed model developed can be used to predict dynamic behavior of the system shown in Fig. 2-1.

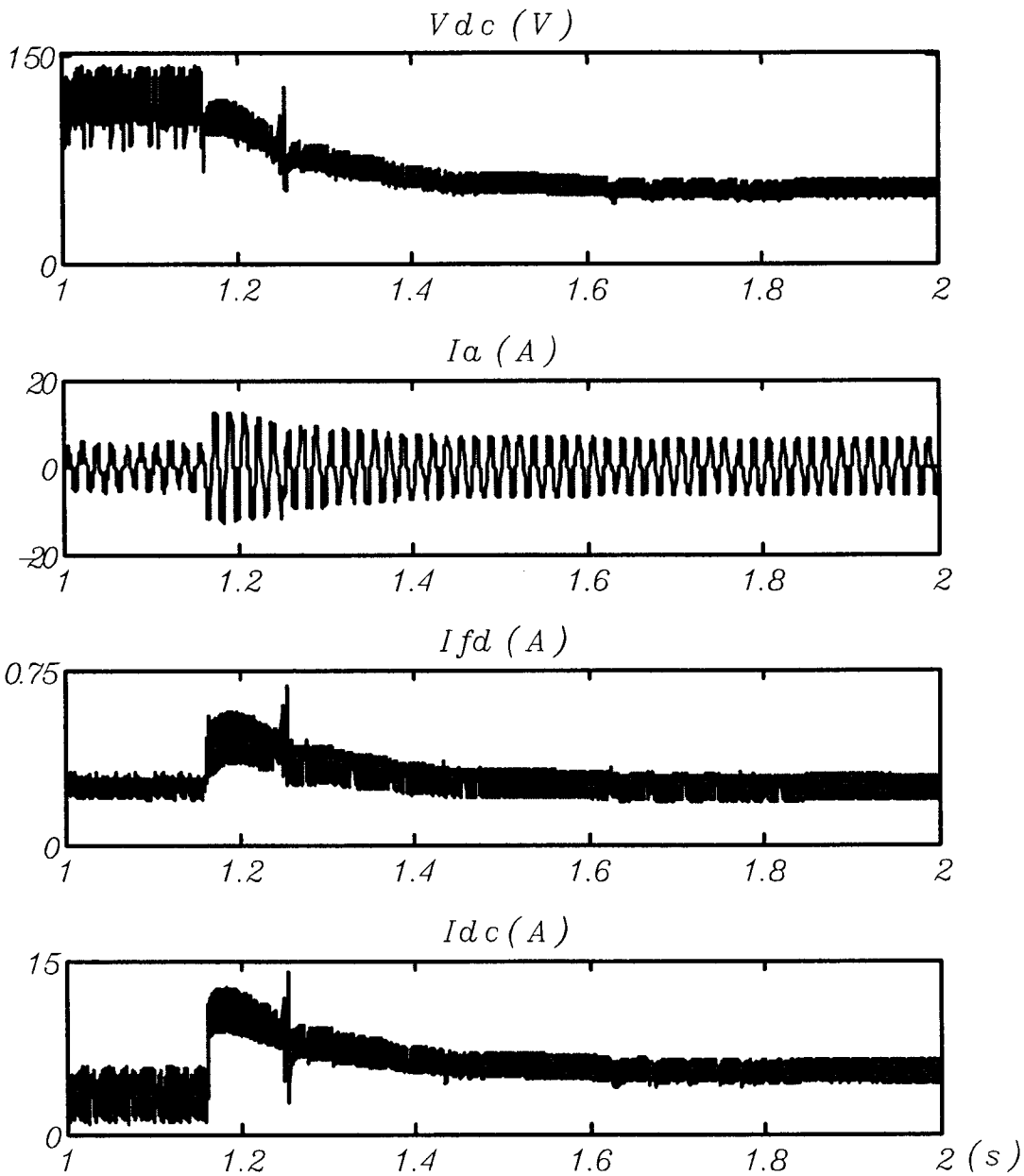

Figure 3-5: Simulation results of the system in Fig. 3.4.

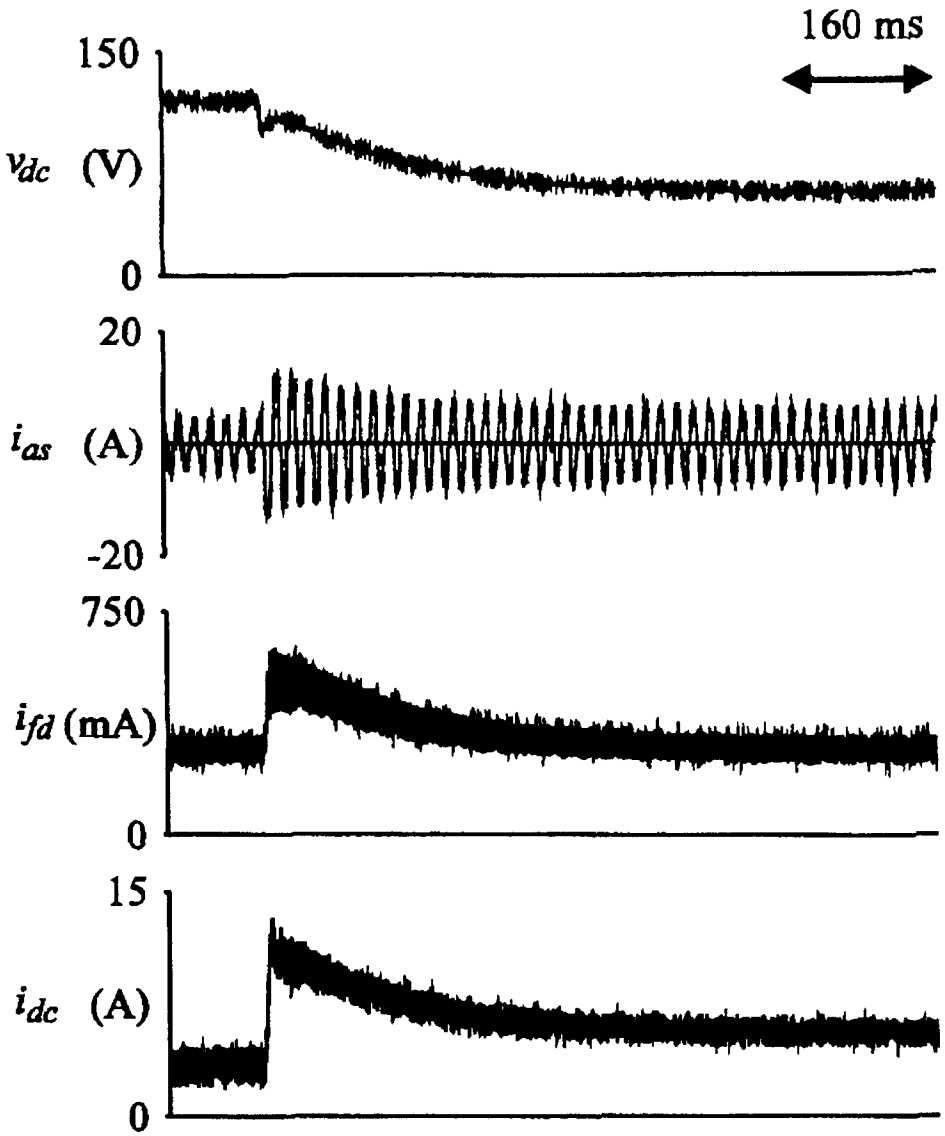

Figure 3-6: Experimental dc-link voltage, a-phase current, field current, and dc-link current from [11] of system in Fig. 3.4.

Chapter 4

Control design

4.1 Overview

It has already been shown that the detailed simulation can be used to predict dynamic behavior of the studied system. The intention of this chapter is to show, in a detailed manner, how control of PCR-ELG was designed based on the results obtained from the detailed simulation.

Two principal control systems directly affect a synchronous generator: the governor and exciter. In order to improve the performance of an isolated power system as discussed in Chapter 1, a firing angle controller of PCR-ELG is considered herein. A feedback loop to the governor is used to maintain the firing angle at its bias value. A simplified view of the control system is expressed diagrammatically in Fig. 4-1, which serves to orient our thinking from the problems of representation of the system to the problems of control. Since usually in power systems, power factor is improved or corrected by deliberately installing capacitor banks, it is assumed that the ac load is resistive. It is also assumed that a reservoir of water exists and is large enough in capacity that, during periods of interest for control analysis, the head is constant. That is to say, the water source is an infinite bus. Referring again to Fig. 4-1, the amount of water power admitted to the hydro turbine is controlled by the governor. PCR-ELG cooperates with the governor to

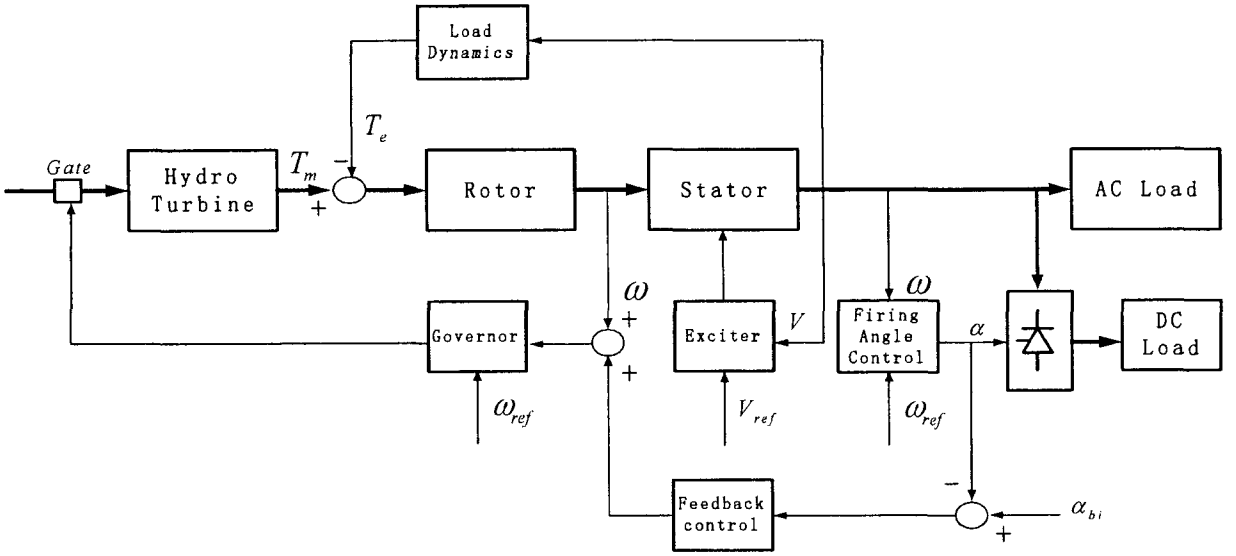

Figure 4-1: Principal controls of the studied system

control the frequency of the system. The firing angle control block adjusts the firing angle quickly to maintain the frequency. If load decreases, the firing angle is decreased by the controller to make PCR-ELG absorb more power. It absorbs less power by increasing the firing angle when load increases. The function of the feedback control is to bring the firing angle back to it bias value to prepare for next disturbance. The excitation system controls the generated EMF of the generator and therefore controls not only voltage but the power factor and current magnitude as well.

4.2 Excitation system

Although to a certain extent, the control of power and frequency is interrelated to the control of reactive power and voltage, the exciter is used primarily as a voltage controller and acts much as a single-input, single-output system with field voltage as the output.

Fig. 4-2 shows in block form the arrangement of the physical components in any excitation system. The voltage regulator is the intelligence in the excitation system

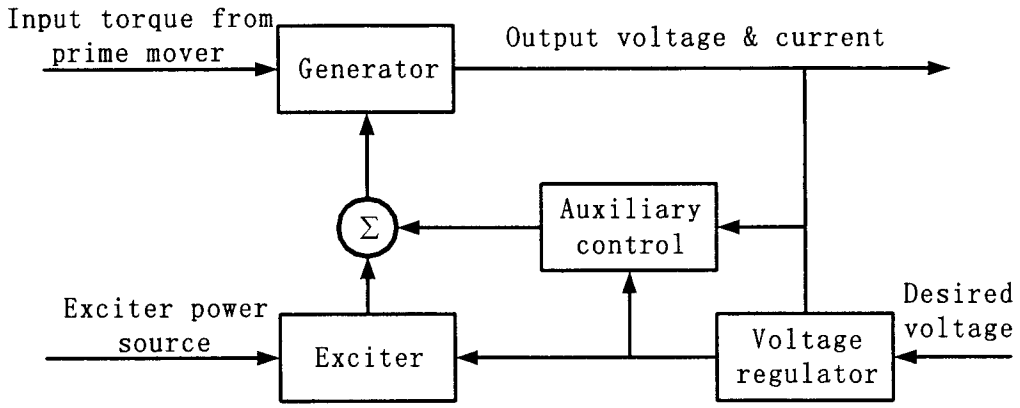

Figure 4-2: Arrangement of excitation components

and controls the output of the exciter so that the generated voltage and reactive power change in the desired way. The voltage regulator is a controller that senses the generator output voltage (and sometime the current) then initiates corrective action by changing the exciter control in the desired direction. In many present-day systems the exciter is a dc generator driven by the turbine (on the same shaft as the generator). An increasing number are solid-state systems consisting of some form of rectifier or thyristor system supplied from the ac bus or from an alternator-exciter. The auxiliary control illustrated in Fig. 4-2 may include several added features. For example, damping is sometimes introduced to prevent overshoot. A comparator may be used to set a lower limit on excitation, especially at leading power factor operation, for prevention of instability due to very weak coupling across the air gap [27].

As the use of computers has increased, IEEE standardized the representation of excitation systems in four different types of models and identified specific commercial systems with each type [18]. These models allow for several degree of complexity, depending upon the available data or importance of a particular exciter in a large system problem. The excitation system models described use a pu system wherein 1.0 pu generator voltage is the rated generator voltage and 1.0 pu exciter voltage is that voltage required to produce rated voltage on the generator air gap line. Type 1 system shown in Fig. 4-3 is used

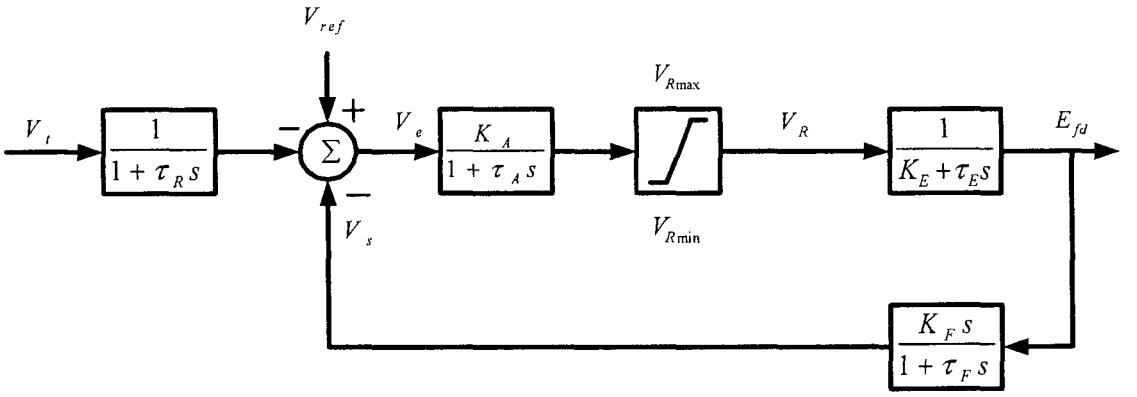

Figure 4-3: Type 1 excitation system representation for a continuously acting regulator and exciter [18]

without the exciter's saturation function in this thesis. Table 4.1 gives a list of symbols used in the IEEE model.

Table 4.1 Excitation System Model Symbols	
E_{fd} exciter output voltage	τ_R regulator input filter time constant
K_A regulator gain	τ_A regulator amplifier time constant
K_E exciter constant related to self-exciter field	τ_E exciter time constant
K_F regulator stabilizing circuit gain	τ_F regulator stabilizing time constant
V_R regulator output voltage	V_s auxiliary (stabilizing) input signal
V_t generator terminal voltage	V_{ref} regulator reference voltage
$V_{R\max}$ maximum value of V_R	$V_{R\min}$ minimum value of V_R

V_t is the generator terminal voltage applied to the regulator input. The first transfer function represents a regulator input filter with time constant τ_R. Usually τ_R is very small and may be considered to zero. The summing point compares the regulator reference with combination of the filter output and the excitation damping loop signal. The main regulator transfer function is represented as a gain K_A and a time constant τ_A. Following this, the maximum and minimum limits of the regulator are imposed so that large input

error signals cannot produce a regulator output which exceeds practical limits. The exciter itself is a first-order linear system with a time constant τ_E and constant K_E as

$$\frac{1}{K_E + s\tau_E} \tag{4.1}$$

Major loop damping is provided by the feedback transfer function

$$\frac{sK_F}{1 + s\tau_F} \tag{4.2}$$

from exciter output to the summing point. The time constant introduces a zero on the negative real axis. Note that (4.2) introduces both a derivative feedback and a first-order lag.

4.3 Speed governing

Because the system studied is a single generator system, the simplest governor, isochronous governor, is used for adjusting the input gate valve to a point that brings frequency back to nominal value. In this kind of hydraulic turbine-generator system, the governing is accomplished by a speed measurement device, a comparator, a controller and one or more force-stroke hydraulic amplifiers. Hydro turbine control was analyzed in [15] by IEEE Working Group on Prime Mover and Energy Supply Models for System Dynamic Performance Studies. This is illustrated as a speed-governing mechanism with the diagram shown in Fig. 4-4. The output of the speed measurement device, ω, is compared with a reference, ω_{ref}, to produce an error signal, $\triangle\omega$. The error is amplified by a gain K_P and integrated with gain K_i to produce a gate position control signal. The force that controls this position error is small and must be amplified in both force and stroke by servomotor, which is modeled by a second-order system. The gate position is limited by the gate opening and speed limit. If, for example, the machine is running at the reference speed and the electrical load increases, ω will fall below ω_{ref} and $\triangle\omega$ will be

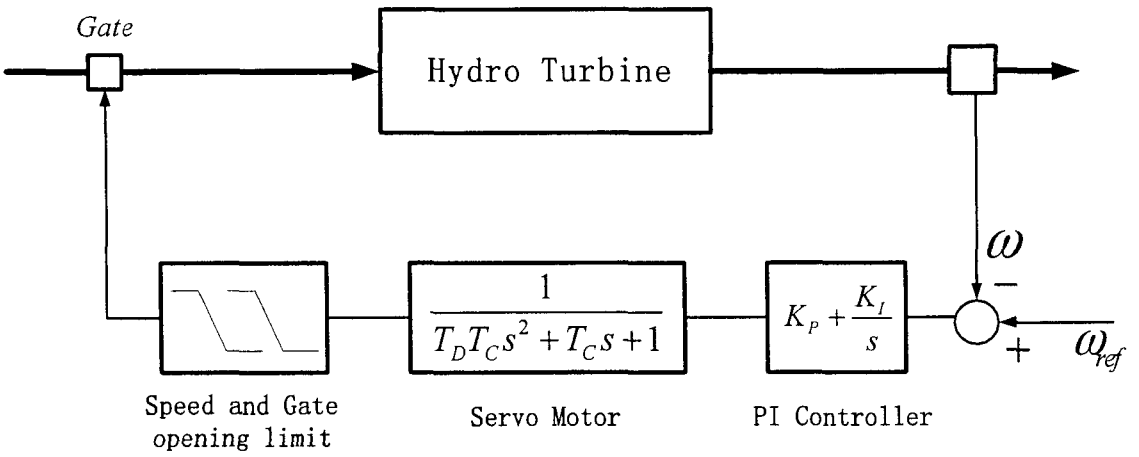

Figure 4-4: Block diagram of hydro turbine isochronous governor

positive. The action of gain and integrator will be to open the gate, causing the hydro turbine to increase its mechanical output, thereby increasing the electrical output of the generator and increasing the speed ω. When ω exactly equals ω_{ref}, the gate stays at the new position (further opened) to allow the generator to meet the increased electrical load.

The isochronous governor cannot be used if two or more generators are electrically connected to the same system since each generator would have to have precisely the same speed setting or they would fight each other. To be able to run two or more generating units in parallel to a generating system, the governors are provided with feedback speed-droop characteristic. This is not investigated in this thesis and is left for consideration in future work.

4.4 PCR-ELG control design

In a power system, it is extremely unlikely that the output of the machines at any instant will exactly equal to the load on the system. If the output of the generators is lower than the demand, the generators will tend to decrease in speed and the frequency will fall,

and vice versa. If the frequency falls by more than 2% the reduced speed of power station pump, fans, etc., may reduce the station output and a serious situation arises. In this type of situation, although the reduction of frequency will cause a reduction in power demand, voltage must be reduced, and if this is not sufficient then loads will have to be disconnected and continue to be disconnected until the frequency rises to a reasonable level or governors adjust power generation. All utilities have a scheme of planned load shedding based on under-frequency relays set to reduce loads in blocks to prevent complete shut-down in extreme emergencies. Even in transient, frequency variation is not allowed beyond 6%.

The electrical dynamics of PCR-ELG are much faster than the mechanical dynamics of hydro turbine governing systems; therefore control of PCR-ELG can be design exclusively by assuming gate opening is constant.

In the system shown in Fig. 4-1, the synchronous generator supplies not only the main ac load but also the dc load through the three-phase controlled rectifier. Neglecting power losses, the power relationship is

$$P_e = P_{ac} + P_{dc} \tag{4.3}$$

where P_e is generator electrical power and P_{ac}, P_{dc} are power absorbed by ac load and PCR-ELG respectively. Then

$$P_{dc} = \frac{V_{dc}^2}{R} \tag{4.4}$$

where R is the dc side resistor. The average dc voltage of ideal 3 phase rectifiers given in Chapter 1 is

$$V_{dc} = \frac{3\sqrt{3}}{\pi} V_p \cos(\alpha) - \frac{3\omega L_s}{\pi} I_{dc} \tag{4.5}$$

Substituting (4.5) in (4.4), we have

$$P_{dc} = \frac{\left[\frac{3\sqrt{3}}{\pi} V_p \cos(\alpha) - \frac{3\omega L_s}{\pi} I_{dc}\right]^2}{R} \tag{4.6}$$

Neglecting $\frac{3\omega L_s}{\pi} I_d$ term, the average dc power can be expressed as

$$P_{dc} = \frac{27}{R}(\frac{V_p}{\pi})^2 \cos^2(\alpha) \tag{4.7}$$

From (4.7), we can see that for a given R, P_{dc} is controlled easily by the firing angle α $(0 < \alpha < \pi/2)$. P_{dc} is a decreasing function of α.

In power systems that include solid-state switching devices such as rectifiers, the time constants associated with the switching devices are on the order of microseconds while the time constants of the excitation and the mechanical dynamics associated with the prime mover may be several seconds. Therefore, the power absorbed by PCR-ELG can be adjusted quickly to the main ac load variation by changing the firing angle, making the overall variation of load very small. For example, if the load decreases, the power going to PCR-ELG can be increased quickly by reducing the firing angle α. This keep the total load almost constant.

4.4.1 Control structure

The controller structure for PCR-ELG is shown in Fig. 4-5. The system frequency, ω, is compared with the reference frequency, ω_{ref}, to produce an error, ω_e. The error is amplified by a gain K_p and integrated to produce a control signal α_c. The control signal α_c and bias firing angle α_{bi} are summed to produce the firing angle α. The maximum and minimum limits of the firing angle are imposed so that large input error signals cannot produce an output which exceeds practical limits. Then a pulse generator can be implemented to fire the thyristors of a six-pulse converter.

4.4.2 Bias firing angle

Phase controlled rectifier with resistive load (PCR-ELG) can operate in rectifier mode with delay angle α greater than 0° but less than 90° (and in inverter mode with delay angle from 90° to 180°). The inverter mode of operation is possible only if a source of

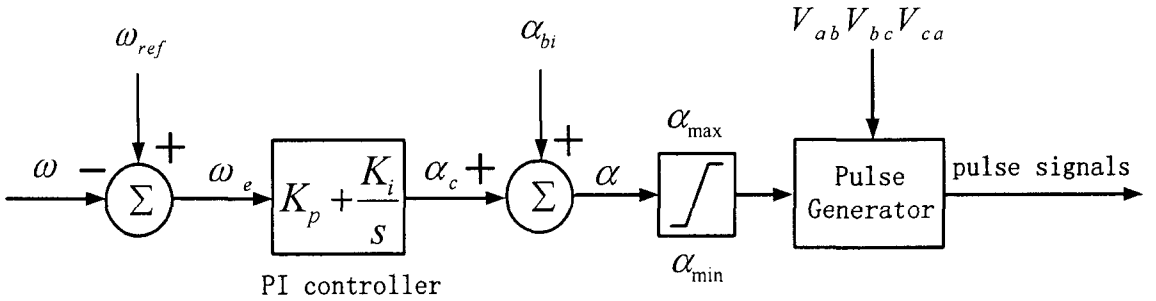

Figure 4-5: Control structure for PCR-ELG

power, such as batteries, is present on the dc side. In this thesis, PCR-ELG is only considered as a load. That means PCR-ELG operates in rectifier mode and the delay angle α lies in the range of 0° to 90°. The maximum and minimum limits of the firing angle are therefore 90° and 0° respectively.

PCR-ELG must absorb certain power in normal situation so that it can reduce or increase the absorbed power to balance the power in the system when the ac load increases or decreases. Accordingly, a bias firing angle needs to be applied to PCR-ELG in normal situation. From (4.7), we can see that P_{dc} is exclusively decided by $\cos^2(\alpha)$. How much power PCR-ELG can absorb or release by changing certain amount of α depends on the slope of a function $y = \cos^2(x)$. As we can see in Fig. 4-6, $y = \cos^2(x)$ has almost same slope from 10° to 80°. A 45° phase angle is a good choice because it has a 45° range on both sides.

4.4.3 DC load determination

PCR-ELG capacity P_{cap} should be greater than or equal to maximum fluctuant load P_f that can be estimated from daily load variation curves. Then the dc side resistor R can be calculated using

$$R = \frac{27}{P_{cap}}(\frac{V_p}{\pi})^2 \cos^2(\alpha_{bi})$$

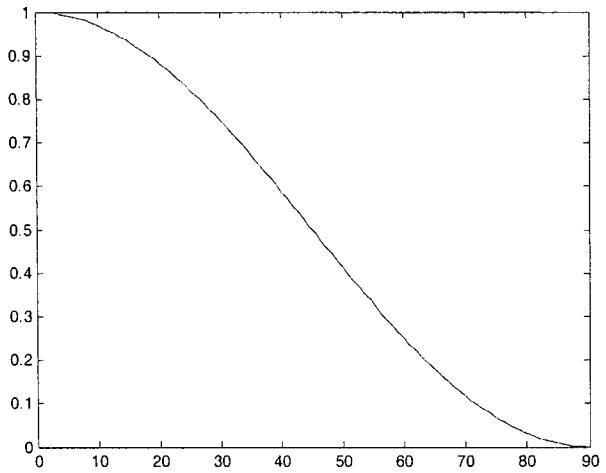

Figure 4-6: y=$\cos^2(x)$

$$\leq \frac{27}{P_f}(\frac{V_p}{\pi})^2 \cos^2(\alpha_{bi}) \tag{4.8}$$

where V_p is fixed for a system and α is chosen as 45°. Maximum value of R can be calculated using (4.8). Dc side resistor R should be chosen smaller than its maximum value to prevent the overshoot of the firing angle exceeds $\frac{\pi}{2}$ or 0. The dc side resistor R can not be too small, otherwise PCR-ELG absorbs too much power during normal situation and it is not efficient.

4.4.4 PI controller tuning

The PI compensator is the simplest compensator that provides zero steady state error. A search for the best set of PI-parameters that gives the desired performance is basically a trial and error process on the models of Chapter 3.

4.4.5 Pulse generator

A synchronized pulse generator can be used to fire the thyristors of a six-pulse converter. The inputs of pulse generators are the firing angle α and three line-to-line converter ac terminal voltages from voltage transformers. The outputs are six pulses individually synchronized on the six thyristor voltages. The pulses are generated α degrees after the zero crossings of the line-to-line voltages.

4.4.6 Control design examples

An example is used to illustrate control design procedures in this section. The controller of PCR-ELG to a system with maximum 20% load disturbance is designed and control results are compared with only using normal governing and excitation system. The system is a hydro turbine synchronous generation unit (300kW) providing power to a village (normally 100kW). The system works at 60Hz and line-to-line voltage is 460V. The specifications of the synchronous generator are given in Table 4.2 [13]. The governor and exciter coefficients from [20] are provided in Table 4.3 and Table 4.4.

Table 4.2 300kW Synchronous Machine Parameters			
$r_s = 0.00285$pu	$X_d = 3.22$pu	$X_q = 2.79$pu	$T'_d = 0.08$pu
$H = 0.1986$pu	$X'_d = 0.21$pu	$X_l = 0.09$pu	$T''_d = 0.019$pu
$P = 2$	$X''_d = 0.14$pu	$X''_q = 0.38$pu	$T''_q = 0.019$pu

Table 4.3 Typical Constants of Hydro Turbine Governors			
$K_a = 3.33$pu	$T_a = 0.07$pu	$\beta = 0$pu	$T_w = 0.6$pu
$g\min = 0.01$pu	$g\max = 0.98$pu	$Vg\min = -0.1$pu	$Vg\max = 0.1$pu
$K_p = 0.6$	$K_i = 0.07$	$K_d = 0$	

Table 4.4 Typical Constants of Excitation Systems		
$\tau_R = 0.02$	$V_{R\max} = 3.5$pu	$V_{R\min} = -3.5$pu
$\tau_A = 0.001$	$\tau_E = 0$	$\tau_F = 0.1$
$K_A = 100$	$K_E = 1$	$K_F = 0.001$

Operation without PCR-ELG

The responses of the system to a step increase in load of 20kW are shown in Fig. 4-7. As can be seen, the gate opening increases from around 33% to 40% of maximum opening due to load increase of 20% while higher field voltage has to be provided to keep the terminal voltage. The phase current changes from 0.33pu to 0.4pu, increasing 20%. The frequency exhibits more than 15% undershoot because 20% disturbance is a very large one for such a small generator. The settling time corresponding to a 1Hz tolerance is about 20s. The simulation results show that normal governing and excitation systems can not provide fine control to the small isolated power system considered.

Operation with PCR-ELG

As in the last section, with a bias firing angle set to 45°, and $\alpha_{\max}$, $\alpha_{\min}$ at 90° and 0° respectively, the maximum load disturbance decides the capacity of the PCR-ELG. Using (4.7) the dc side resistor R can be calculated as

$$\begin{aligned} R &\leq \frac{27}{P_f}(\frac{V_p}{\pi})^2 \cos^2(\alpha) \\ &\leq 9.65\Omega \end{aligned}$$

This means that R should be no more than 9.65Ω if PCR-ELG is required to have enough capacity to absorb/release 20kW load. As discussed in last section, overshoot of α and power absorbed by PCR-ELG during normal situation need to be considered.

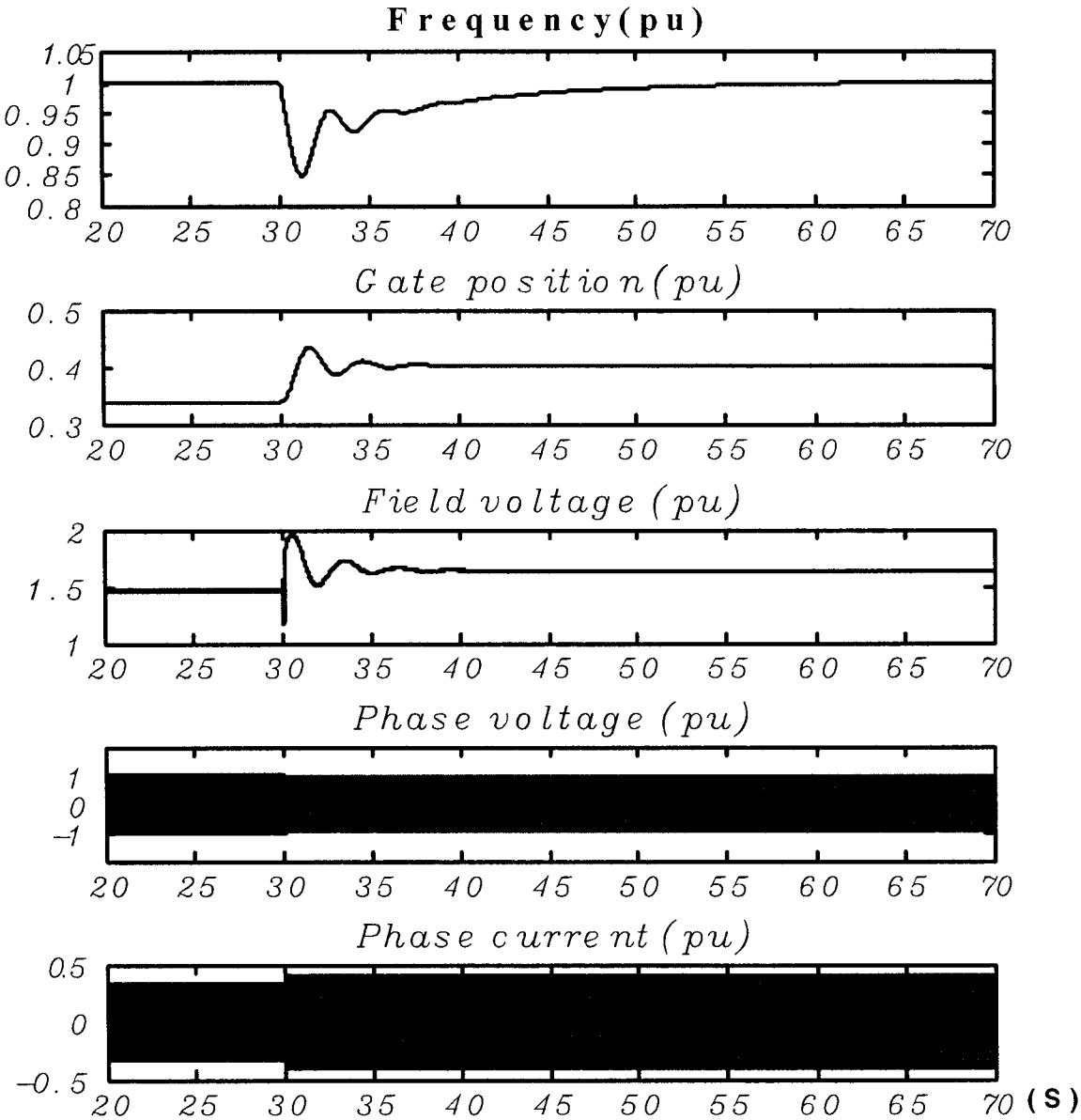

Figure 4-7: The system responses to a step in load disturbance of 20kW without PCR-ELG

Here R is chosen as 8Ω and an inductor of 0.02H is used in series with the resistor as stray inductance. In this case, K_p is chosen as 10 and K_i as 25 per sec as controller parameters.

Fig. 4-8 show the responce with PCR-ELG to 20kW load disturbance. As shown in Fig. 4-8, both firing angle and gate opening respond to load increase immediately. Because the electrical dynamics of PCR-ELG is much faster than the mechanical dynamics of hydro turbine governing system, PCR-ELG play the main role of power control in the system to maintain the frequency. As a result, dc average voltage reduces and consequently dc side current decrease from 53A to 19A while the output average power barely changes. Due to the control effect of PCR-ELG the system frequency can be kept within 0.7% and reach its steady state in about 2s.

Compared with hydro turbine governor, PCR-ELG obviously provides much better control to the system.

4.5 Feedback loop control design

As can be seen from Fig. 4-8, the firing angle settles down to around 72° in steady state. The firing angle α lies in the range of 0° to 90°. If loads are changing for a sustained duration, the firing angle of rectifier needs to be cut back to the bias angle to prepare for next disturbance. Coordinated control of the turbine and electronic load governor is necessary to make PCR-ELG have continuable control capability. This can be accomplished by adding a feedback loop from the firing angle to input frequency of the governor as shown in Fig. 4-1.

4.5.1 Control structure

From Fig. 4-8, after PCR-ELG controls the frequency to its rated value, the speed error is zero and the gate opening stays almost constant. If we want the generator to provide more power so that the firing angle can go back to its bias value for next disturbance, a

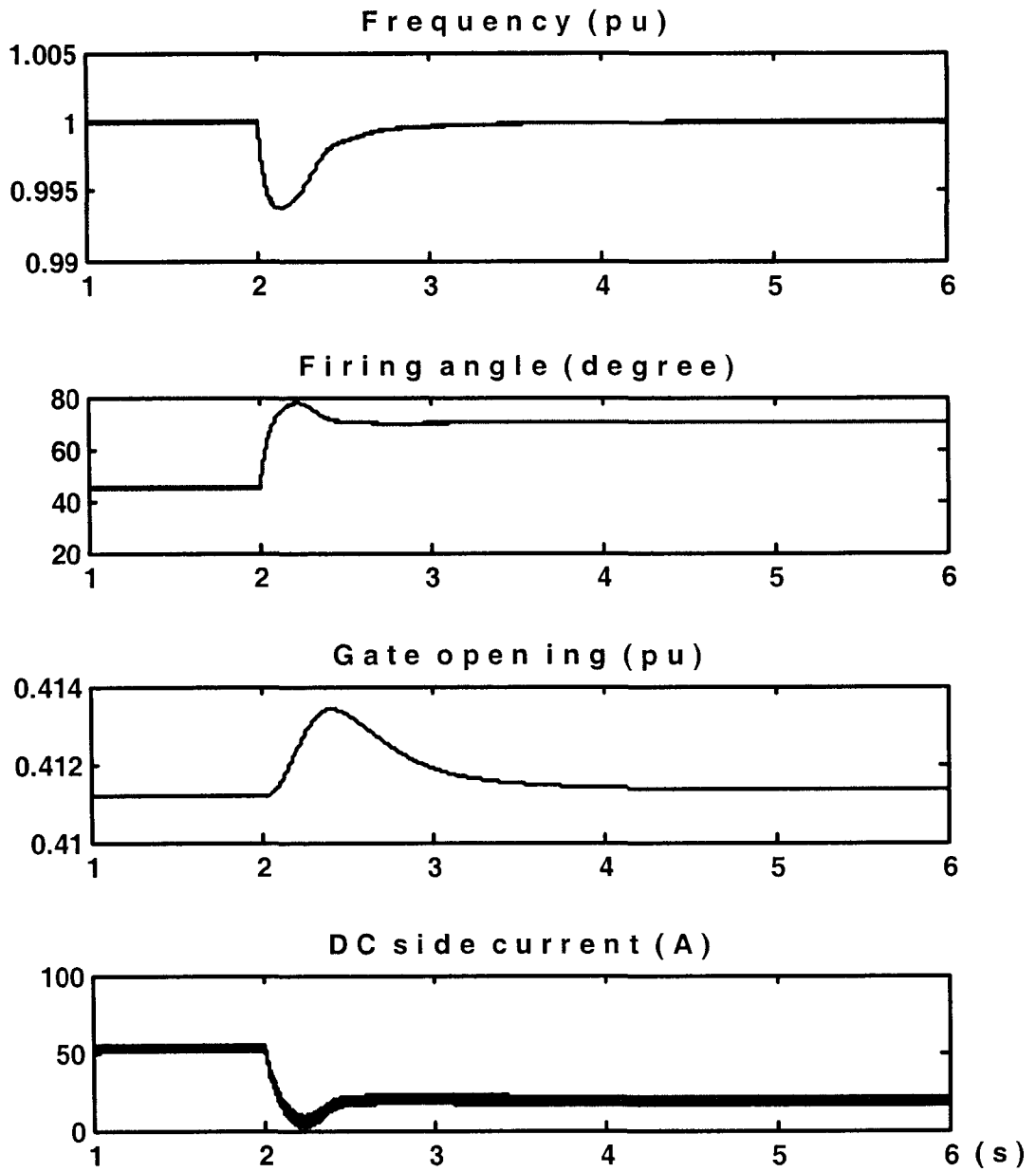

Figure 4-8: Response of frequency, firing angle, gate opening and DC side current to 20kW load disturbance with PCR-ELG

fake speed error signal has to be imposed to the governor. Therefore a pseudo angular velocity ω_{pse} is considered. The feedback loop structure is designed as shown in Fig. 4-9. The error between the firing angle and its bias value is amplified by a positive feedback gain k and added to the system speed to produce a pseudo angular velocity ω_{pse}, which is compared with the reference speed to obtain speed error ω_e. Pseudo angular velocity ω_{pse} is given by

$$\omega_{pse} = \omega + k(\alpha_{bi} - \alpha) \tag{4.9}$$

From Figures 4-7 and 4-8, it can be seen that settling time of the system without PCR-ELG is longer than that with PCR-ELG by a factor of up to 15. The electrical dynamics of PCR-ELG are much faster than the mechanical dynamics of hydro turbine governing system. Therefore PCR-ELG and hydro turbine governing system can be considered separately for the convenience of analysis. In the first period of time before the system frequency is brought back to its reference value by PCR-ELG, the effect of governor and feedback loop can be neglected. If loads increase, the system frequency can be brought back to a reference frequency very quickly due to the effect of PCR-ELG. The firing angle however increases (for an ac load increase) to a certain value. After the system frequency has settled down, the effect of governor and feedback loop is considered with assumption of rated system speed ω. When ac load increases, the firing angle increases. Referring to (4.9), the increase in α causes ω_{pse} to be lower than the system reference speed (Fig. 4-9) and speed error ω_e is positive. This positive error makes the gate open further increasing generated power. The firing angle of PCR-ELG will reduce to absorb this increase in generated power. This procedure will continue until the system reach its steady state in which the firing angle and the system frequency equal to their reference values respectively. Referring to (4.9) again, ω_{pse} equals the reference angular velocity ω_{ref} and speed error ω_e is zero in steady state along with $\alpha = \alpha_{bi}$.

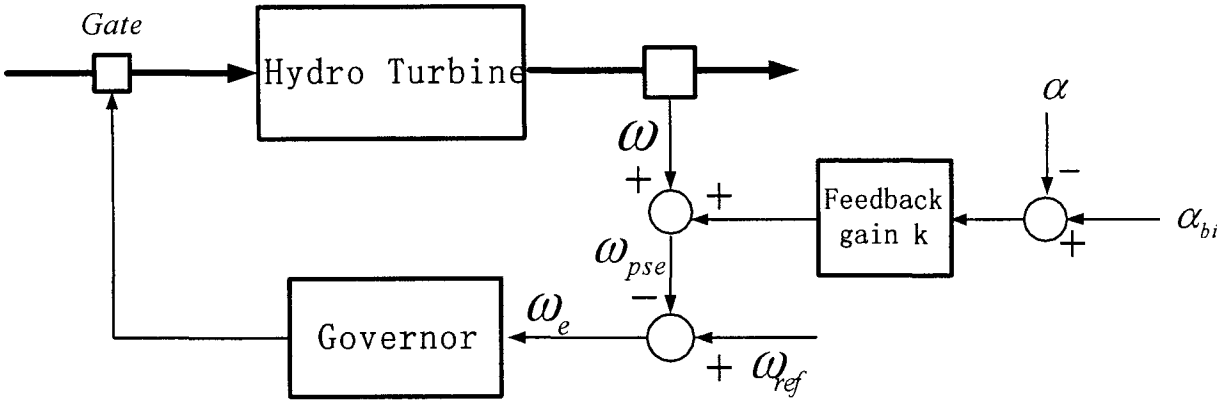

Figure 4-9: Feedback loop structure

4.5.2 Feedback loop gain determination

As mentioned, the electrical dynamics of PCR-ELG are much faster than the mechanical dynamics of hydro turbine governing systems; therefore feedback loop gain can be decided by assuming rated constant system frequency. From Fig. 4-7, undershoot of the frequency is 16% without PCR-ELG. This means an absolute maximum speed error of 16% can be tolerated in the governor to bring the firing angle back to its bias value after PCR-ELG controls the frequency. Referring to Fig. 4-9, when the system frequency ω equals to reference frequency ω_{ref},

$$k\,|\alpha_{bi} - \alpha| = |\omega_e| \leqslant 0.16$$

The firing angle α lies in the range of 0° to 90°. With $\alpha_{bi} = \frac{\pi}{4}$,

$$|\alpha_{bi} - \alpha| < \frac{\pi}{4} \approx 0.78$$

Therefore the feedback loop gain k should be not more than $0.16/0.78 \approx 0.2$. Pseudo angular velocity ω_{pse} should not produce too large speed error ω_e, otherwise the governor and PCR-ELG would fight each other, each trying to pull the system frequency to its own setting. This would cause oscillations in the system frequency. This can be seen in

the following simulations.

4.5.3 Control design examples

Operation with a feedback loop gain of 0.15

The same system as in subsection 4.4.6 is used here for control design. The feedback gain k is set to 0.15. The system with PCR-ELG as well as the feedback loop is simulated for an ac load increase from 100kW to 120kW and an ac load decrease from 100kW to 80kW. The results are shown in Figs. 4-10 and 4-11 respectively. Due to the control effect of PCR-ELG the system frequency can be kept within $\pm 0.8\%$ and reach its steady state in about 5s. Because of existence of the feedback loop, the gate opens further even when the system frequency is already controlled to its reference value. As a result, the firing angle and dc side current go back to their values before the load change in the steady state.

There are oscillations in the gate opening waveforms. In practice, theses oscillations can cause equipment malfunction. This is because the feedback loop produces too large pseudo speed error and the governor and PCR-ELG fight each other, each trying to pull the system frequency to its own setting. A smaller feedback loop gain needs to be used to eliminate these oscillations.

Operation with a feedback loop gain of 0.05

The simulation results in Figs. 4-12 and 4-13 show that oscillations can be eliminated by choosing a smaller value of a feedback loop gain. With the effect of PCR-ELG as well as the feedback loop, the overshoot of frequency is not more than 0.7%. The frequency settles down within 2s. Firing angle can come back to its bias value in the steady state and the oscillations of the earlier simulations in Figs. 4-10 and 4-11 are greatly reduced in Figs. 4-12 and 4-13.

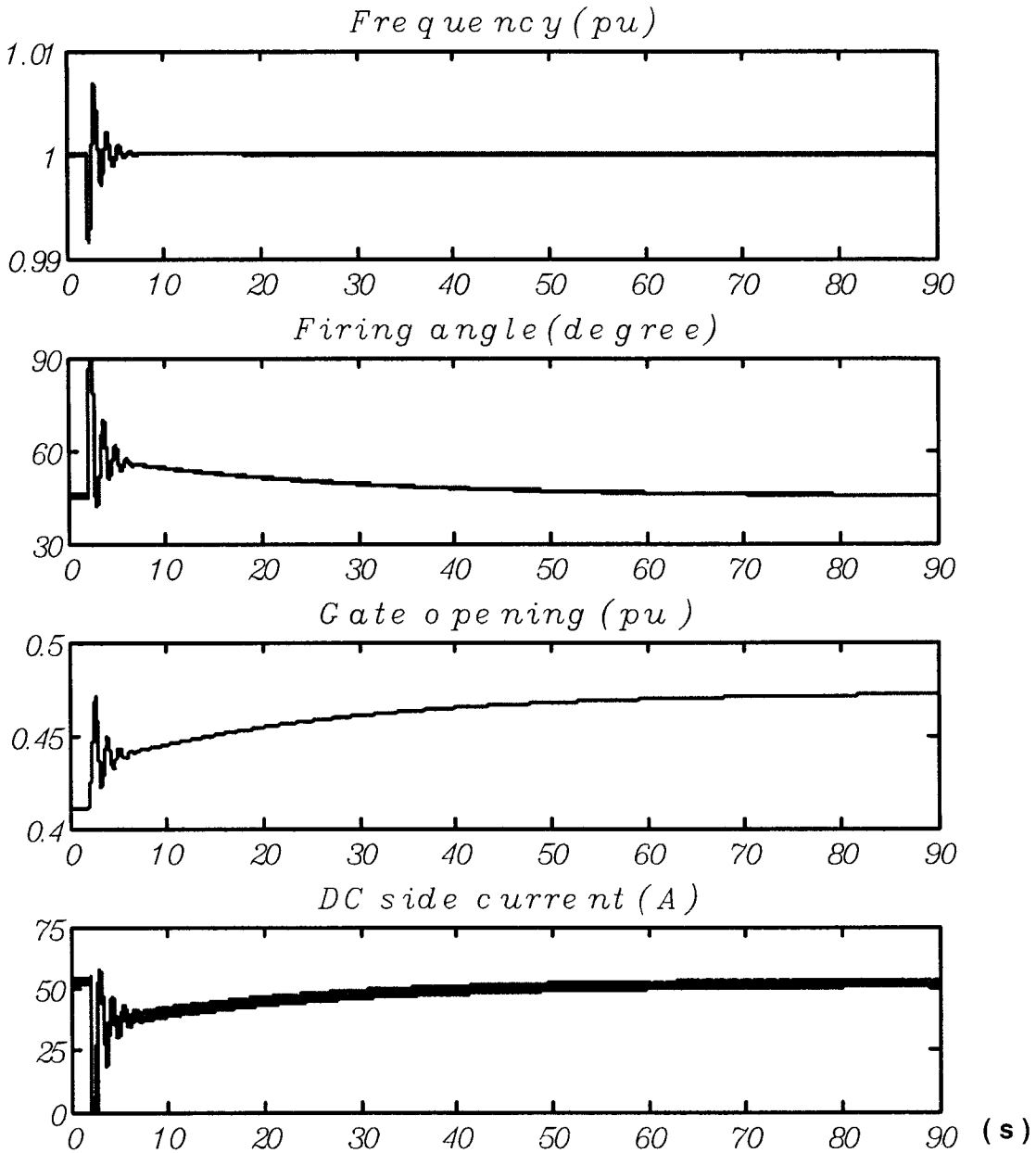

Figure 4-10: Response to 20kW load increase with PCR-ELG and feedback loop gain at 0.15

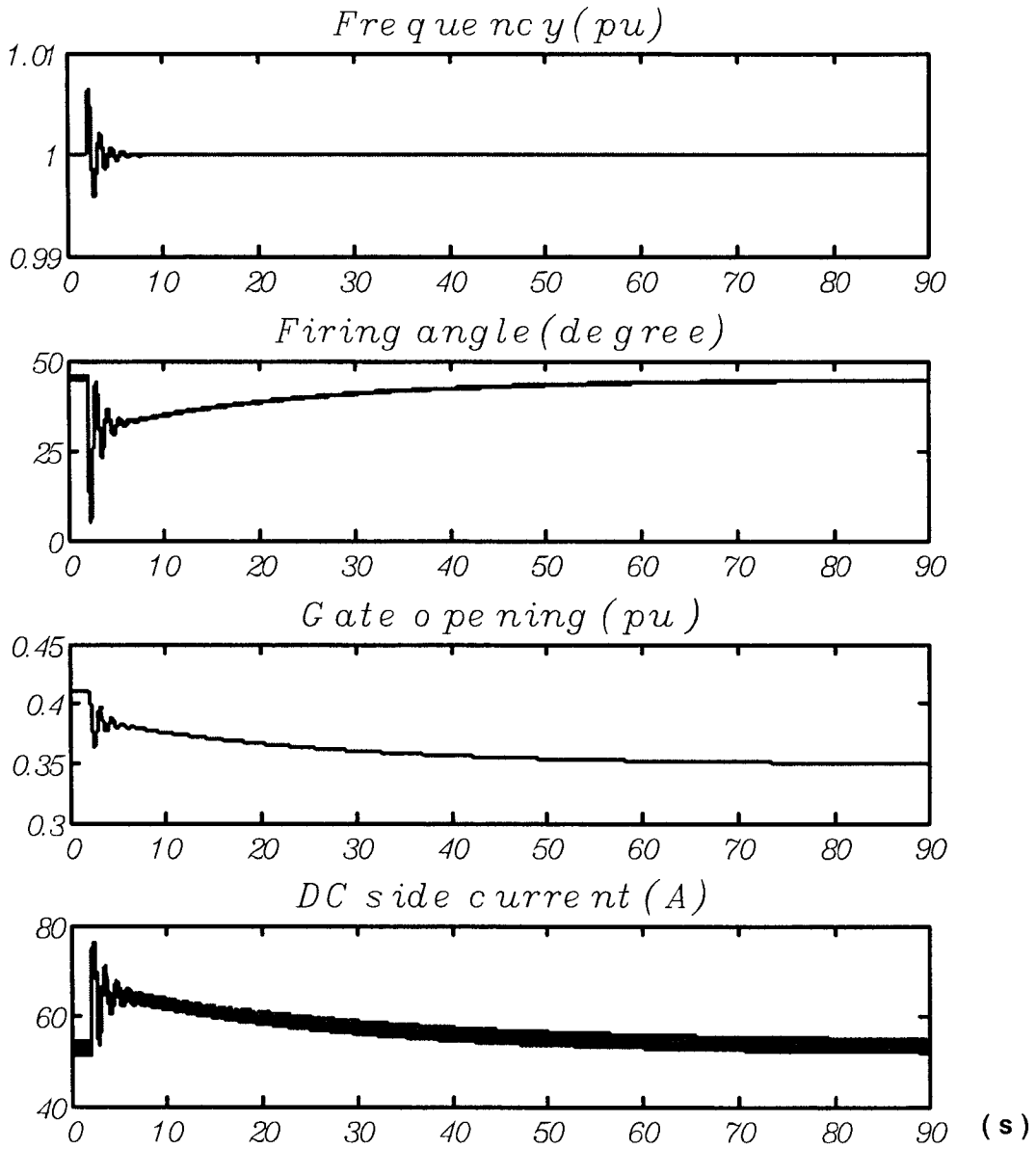

Figure 4-11: Response to 20kW load decrease with PCR-ELG and feedback loop gain at 0.15

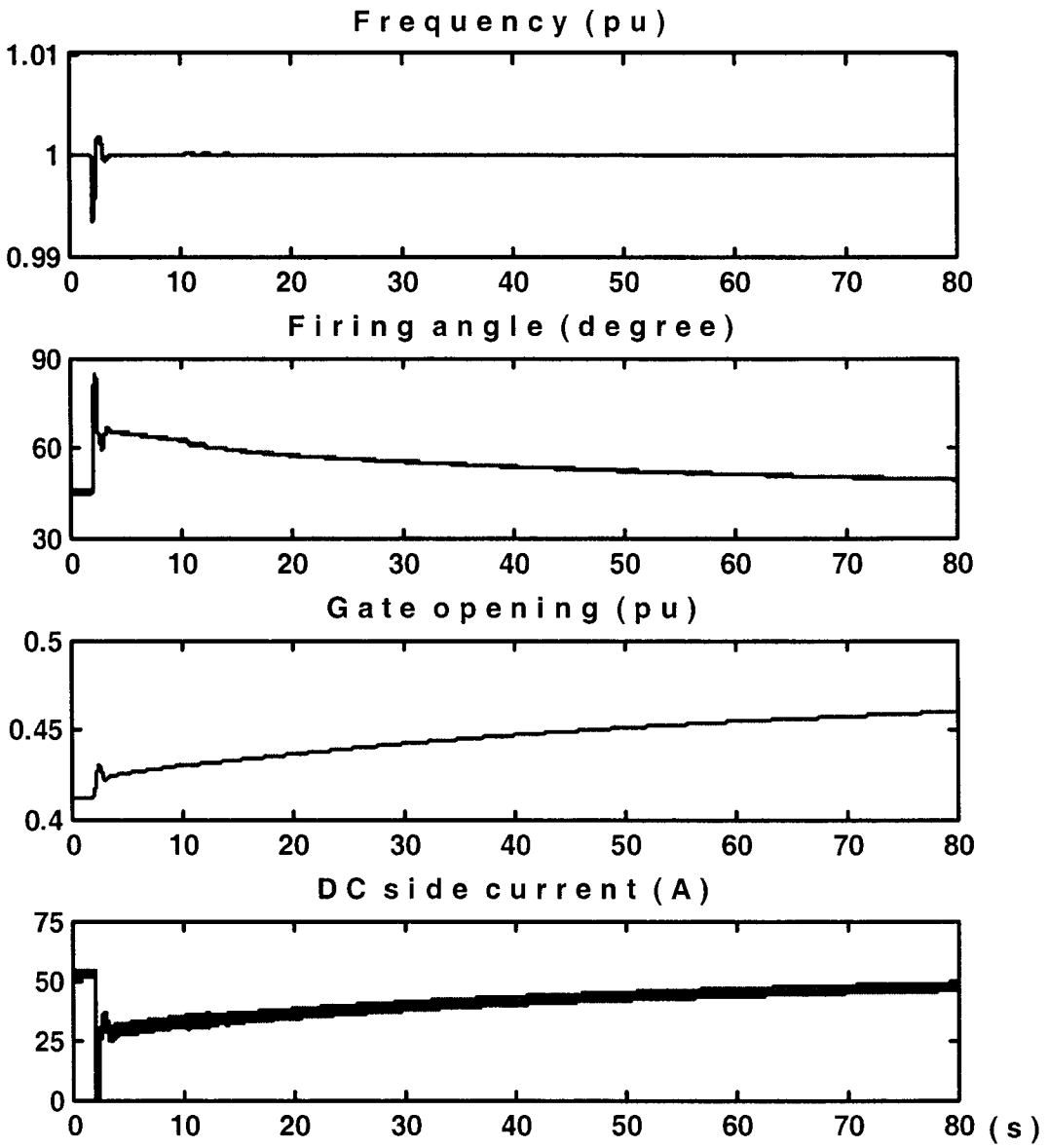

Figure 4-12: Response to 20kW load increase with PCR-ELG and feedback loop gain at 0.05

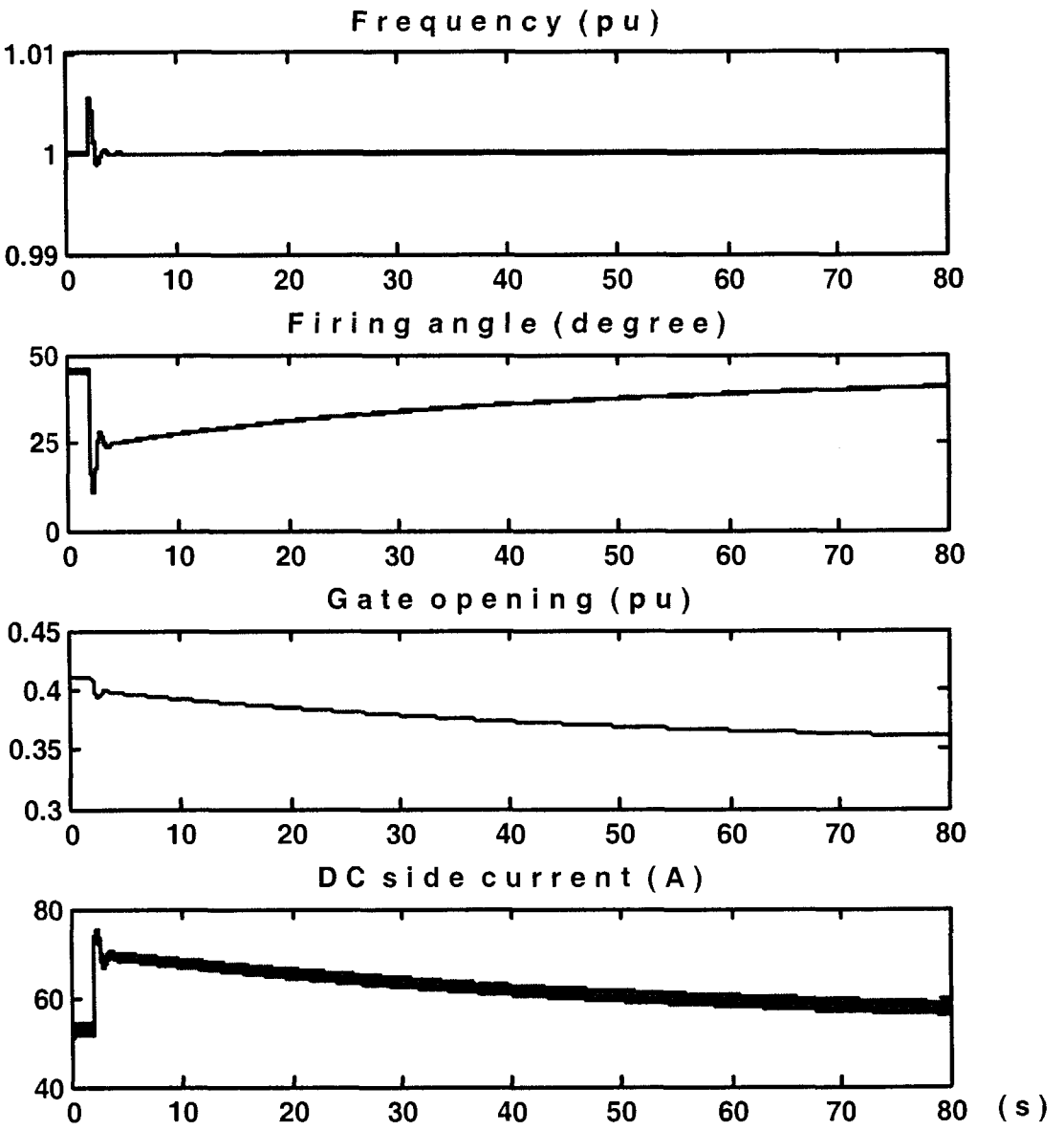

Figure 4-13: Response to 20kW load decrease with PCR-ELG and feedback loop gain at 0.05

Chapter 5

Conclusion

5.1 Summary and Conclusions

Due to the need of fine frequency control for an autonomous power system, this thesis presents a design concept of an electronic load governor (ELG) which is used to absorb fast load variations to maintain the autonomous network frequency within tight specifications.

The basis for development of the simulations in the thesis consists of models of synchronous generators, hydro turbines, rectifiers and ac load. These models are available in the literature. Matlab/Simulink with the SimPowerSystems package is used to interface each component. The ac and dc side waveforms from the simulation are compared with experimental results in the literature to verify the simulation. The results show that they are quite consistent with each other. How the PCR-ELG affects the ac waveforms is presented through the analysis of terminal voltage and current of the generator. It can be concluded from such analysis that terminal voltage and current of the generator are distorted because of the current commutation of the controlled rectifier. Based on the simulation's results, the control design of PCR-ELG with feedback loop is carried out. Governing and excitation system widely used in industry are introduced for the purpose of the comparison with PCR-ELG control with feedback to governor loop. The design of the firing angle by PI controller for the PCR-ELG along with feedback loop is given

in detail and examples are used to show advantages of PCR-ELG control over normal governor system. The frequency of an autonomous power system can be controlled within $\pm 1\%$ even with a very large disturbance while a $\pm 16\%$ variation of frequency is observed when using normal governor system without the PCR-ELG. PCR-ELG control can make the frequency settle down to almost 1 pu within 2 seconds, 10 times shorter than in the normal governor system.

The frequency control results using the PCR-ELG along with feedback loop are much better than those in [1] using ZC-ELG. As mentioned, the frequency of an autonomous power system can be controlled within $\pm 1\%$ with 20% load change. In [1], a full load rejection causes the frequency rising about 20% at its peak. In addition, ZC-ELG was not cooperated with the governor of a synchronous generator in [1]. Hence it did not have continual control capability.

5.2 Future Research

As can be seen from the simulation and experimental results, the generator's terminal voltages and currents are distorted by the current commutation of the controlled rectifier. Therefore, a filter on the ac side to reduce the harmonics is a subject of future investigation. Coordination of the scheme with composite generation system such as a mini-hydro turbine and diesel generation system should also be investigated.

Bibliography

[1] D.S. Henderson, "An Advanced Electronic Load Governor for Control of Micro Hydro Electric Generation," IEEE Trans. Energy Conversion, Vol. 13, No. 3, pp. 300-304, Sept. 1998.

[2] W.J. Bonwick and V.H. Jones, "Rectifier-Loaded Synchronous Generators with Damper Windings," Proceedings of the Institution of Electrical Engineers, Vol. 120, No. 6, pp. 659-666, Jan.-June 1973.

[3] M. Goto, A. Yokoshima and A. Isono, "Transient Behavior of Synchronous Machines with Thyristor Converter Loads," Electrical Engineering in Japan, Vol. 99, No. 5, pp. 86-95, Sep.-Oct. 1979.

[4] S. Moriyasu, C. Uenosono and Kawasaki, "An Analysis on the Characteristics of a Synchronous Machines Connected to a d.c-link," Archiv fuer elektrotechnik (Berlin), Vol. 69, No. 2, pp. 111-120, 1986.

[5] N. Mohan, "Power Electronics: Converters, Applications, and Design," John Wiley and Sons, 2003.

[6] J.G. KettlebOrough, I.R. Smith and B.A. Fanthome, "Simulation of a Dedicated Aircraft Generator Supplying a Heavily Rectified Load," IEE Proceedings, vol. 130, No. 6, pp. 431-435, Nov. 1983.

[7] T.H. Wamer and J.G. Kassakian, "Transient characteristics of Large Turboalternator Driven Rectifer/Inverter Systems Based on Field Test Data," IEEE Trans. on Power Apparatus and Systems, Vol. 104, No. 7, pp. 1804-1811, July 1985.

[8] IEEE Committee Report, "Proposed Excitation System Definitions for Synchronous Machines," IEEE Trans. on Power Apparatus and Systems, Vol. 88, No. 8, pp. 1248-1258, Aug. 1969.

[9] I. Jadric, "Modeling and Control of a Synchronous Generator With Electronic Load," IEEE Trans. Power Electronics, Vol. 15, No. 2, pp. 303-309, March 2000.

[10] S. Sudhoff and O. Wasynczuk, "Analysis and Average-Value Modeling of Line-Commutated Converter-Synchronous Machine System," IEEE Trans. Energy Conversion, Vol. 8, No. 1, pp. 92-99, March 1993.

[11] J.T. Alt and S. Sudhoff, "Analysis and Average-Value Modeling of an Inductorless Synchronous Machine Load Communtated Converter System," IEEE Trans. Energy Conversion, Vol. 14, No. 1, pp. 37-43, March 1999.

[12] W. Ma, A. Hu and G. Zhang, "Stability of a Synchronous Generator with Diode-Bridge Rectifier and Back-EMF Load," IEEE Trans. Energy Conversion, Vol. 15, No. 4, pp. 458-463, Dec. 2000.

[13] The MathWorks, "SimPowerSystems User's Guide Version 4.1".

[14] MGA software, Concord, "ACSL Reference Manual Edition 11.1".

[15] IEEE Working Group on Prime Mover and Energy Supply Models for System Dynamic Performance Studies, "Hydraulic Turbine and Turbine Control Models for Dynamic Studies," IEEE Trans. Power System, Vol. 7, No. 1, pp. 167-179, Feb. 1992.

[16] R.E. Doan and K. Natarajan,"Modeling and Control Design for Governing Hydroelectric Turbines with Leaky Wicket Gates," IEEE Trans. Energy Conversion, Vol. 19, No. 2, pp. 449-455, June 2004.

[17] K. Natarajan, "Robust PID Controller Design for Hydroturbines," IEEE Trans. Energy Conversion, Vol. 20, No. 3, pp. 661-667, Sept. 2005.

[18] IEEE Committee Report, "Recommended Practice for Excitation System Models for Power System Stability Studies," IEEE Standard, 1992.

[19] P. Krause, O. Wasynczuk and S. Sudhoff, "Analysis of Electric Machinery and Drive Systems," Wiley-Interscience, 2002.

[20] P.M. Anderson and A.A. Fouad, "Power System Control and Stability," Wiley-Interscience, 2003.

[21] R.H. Park, "Two-Reaction Theory of Synchronous Machines-Generalized Method of Analysis, Part I," AIEE Transactions, Vol. 48, pp. 716-727, July 1929.

[22] R.H. Park, "Two-Reaction Theory of Synchronous Machines, Part II," AIEE Transactions, Vol. 52, pp. 352-355, June 1933.

[23] J. Doval-Gandoy and C. Castro, "Analysis of a Current Source Rectifier In Transient And Steady State," IECON Proceedings, Vol. 1, pp. 354-359, 1999.

[24] C.M. Ong, "Dynamic Simulation of Electric Machinery," Prentice-Hall PTR, 1998.

[25] R.J. Harrington and S.A. Gawsih, "A Digital Computer Model of Three-phase Rectifier/inverter Systems for Transient Studies," Proceedings of Power electronics and applications, Vol. 1, pp. 2131-2136, 1985.

[26] S. Sudhoff, "Waveform Reconstruction from the Average-Value Model of Line-Commutated Converter Synchronous Machine Systems," IEEE Trans. Energy Conversion, Vol. 8, No. 3, pp. 404-410, Sept. 1993.

[27] C. Concordia and M. Temoshok, "Generator Excitation Systems and Power System Performance," IEEE Summer Power Meeting, Portland, Oreg., pp. 31 CP 67-536, 1967.